Journal of The Electrochemical Society

Review—Recent Advances in Graphene-Based Field-Effect-Transistor Biosensors: A Review on Biosensor Designing Strategy

Journal of The Electrochemical Society, 2022 **169** 027509
1945-7111/2022/169(2)/027509/18/$40.00

Review—Recent Advances in Graphene-Based Field-Effect-Transistor Biosensors: A Review on Biosensor Designing Strategy

Shuo Wang,[1] Xin Qi,[1] Danni Hao,[1] Ramiro Moro,[1] Yanqing Ma,[1,2,z] and Lei Ma[1,z]

[1]*Tianjin International Center for Nanoparticles and Nanosystems, Tianjin University, Tianjin 300072, People's Republic of China*
[2]*State Key Laboratory of Precision Measuring Technology and Instruments, Tianjin University, Tianjin 300072, People's Republic of China*

Biosensors for quick diagnosis and in situ monitoring are increasingly needed in health care. Field-effect transistor (FET) based biosensors have attracted much attention due to their high sensitivity and compatibility with point-of-care applications. As the most important 2D material, graphene has been investigated intensively as a channel material for transistor-based sensors due to its easily enhanced selectivity by rather simple functionalization. However, in order to realize its practical applications, challenges still remain, such as device stability and reproducibility. Here, we review recent progress in the general design strategy of high-performance graphene field-effect transistor (GFET) biosensors with emphasis on the device physics, defects, Debye screening, and functionalization. Finally, both current applications and perspectives on future development are given.
 [DOI: 10.1149/1945-7111/ac4f24]

Manuscript submitted October 9, 2021; revised manuscript received January 22, 2022. Published February 16, 2022.

Field-Effect-Transistors (FETs) based biosensors are promising biochemical sensing platforms, which are compatible with point-of-care applications due to their potential for highly sensitive, label-free, real-time selective detection and their ability to be integrated into electronic manufacturing processes for achieving "lab-on-a-chip".[1,2] The conventional transduction capabilities of FETs based biosensors rely on the fact that the conductance of their channel material is determined by the amount of absorbed target molecules and their gating properties.[3] The intrinsic electronic properties and bio-recognition process of the channel materials determine the performance of the biosensors including the sensitivity, selectivity, and stability.[4]

Early FET sensors used traditional semiconductors (e.g. silicon, stannic oxide) as the channel material, they had low sensitivity and require strict detection conditions.[5] Besides, with minimization of their sizes, the available channel materials are vastly limited due to the largely increased leakage current between source and drain[6] and consequently the static power consumption. Moreover, scattering of charge carriers caused by dangling bonds will further deteriorate the FETs' performance.[7,8] To achieve high-performance FET based biosensors, many low-dimensional nanomaterials have been tested as potential channels.[9,10]

Compared with a bulk semiconductor material, all atoms of low-dimensional materials are on the surface, making them highly sensitive to any interaction with their surrounding environment. In addition, some low-dimensional materials have more stable and superior electrical properties as FET channels compared to the conventional bulk materials. As typical examples, silicon nanowires (SiNWs) and carbon nanotubes (CNTs) based sensors that have demonstrated great sensitivity.[11] However, their complex and unscalable fabrication procedures make them far from practical applications.[12]

On the other hand, graphene has been studied extensively ever since it was revived back nearly 20 years ago due to its remarkable physicochemical properties.[13,14] Benefit from its large 2D lateral planar size, graphene can form an ideal electrical contact with the metal electrodes and this makes it more suitable for manipulating the channel structure combine with the microfabrication process, which is hard to achieve with one-dimensional materials. Considering its superior carrier mobilities up to 10^6 cm^2 V^{-1} s^{-1} at room temperature,[15–17] which is almost 3 orders of magnitude higher than traditional semiconductor materials like silicon (~1500 cm^2 V^{-1} s^{-1})[18,19] and other 2D layered materials like molybdenum disulfide (MoS_2)(~60 cm^2 V^{-1} s^{-1} at 250 K).[20] Graphene was conceived as one of the most idealistic materials for ultra-fast sensors.[4,12] Besides, the honeycomb carbon network of graphene formed through sp^2 hybridization makes it structurally stable and chemically inert[21] and provides an extremely high surface-to-volume ratio. The easiness of functionalization of the graphene surface greatly benefits bio-recognition and further offers a broad band of approaches for enhancing the selectivity of graphene based sensors,[22] even superior to those of SiNWs and CNTs. Hence, GFET biosensors exhibit an achievable limit of detection (LOD) falling in the range of pico-molar (pM) to femto-molar (fM). With proper processing techniques, it is possible to further push this limit to the atto-molar (aM) range.[23] It has been applied to detect traces of various human-based biomarkers which has provided an avenue to realize portable and wearable sensors with real-time clinical surveillance.[24–26] Recently, it has been further extended to monitor human physiological status.[27] Although well-designed GFET biosensors have been applied in various forms for biomolecule detection, there is still room for sensor performance improvement. Therefore, it is necessary to make a brief summary of the latest progress for updating the development of GFET biosensors and their applications.

Here, we present an overview of the strategies in constructing GFET biosensors and summarize the current applications, as well as perspectives on future development. Although reduced graphene oxide (rGO) are widely used in FET biosensors applications,[28,29] there is still a large room to be improved due to their rather low mobility (FET based on rGO with a mobility on the order of 10 cm^2 V^{-1} s^{-1} or even less[30,31]) and high noise level caused by a large number of oxygen-containing defects introduced by the redox process.[32] Moreover, there is absence of effective methods to completely remove these oxygen-containing groups,[33] leading to a low controllability of defects. We omit the studies of GFET biosensors based on rGO as they are covered extensively elsewhere.[24,25,34–36] We adhere to the principles of achieving better electrical conductivity and low detection limits, dedicate to summarizing the research on the preparation of FET biosensors based on high-quality graphene.

Fundamental Physics of GFETs

As shown in Fig. 1a, the typical structure of a GFET biosensor consists of a graphene channel between source and drain electrodes on an insulating substrate. Since biosensors primarily operate in a liquid environment, the gate voltage is applied through an immersed metallic electrode or electrochemical reference electrode. The source and the drain electrodes are usually coated with an insulator layer to electrically segregate them from the gate electrode. By changing the

[z]E-mail: mayanqing@tju.edu.cn; lei.ma@tju.edu.cn

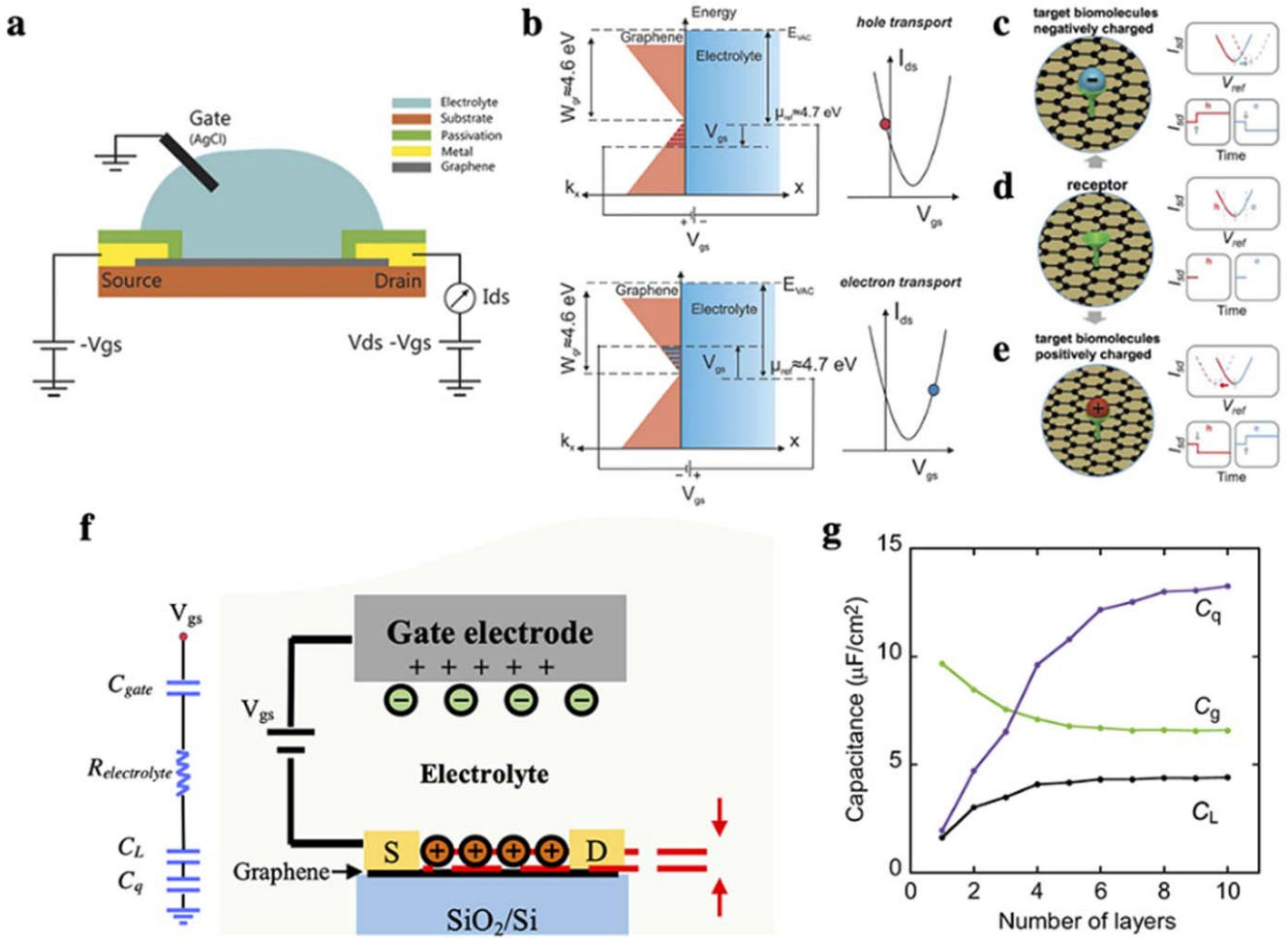

Figure 1. (a) The cross-sectional scheme of the graphene solution-gated FET biosensor. (b) A momentum-energy illustration of the graphene-solution interface. The Ag/AgCl reference electrode with an electrochemical potential around 4.7 eV is used as the gate electrode. The work function of graphene is around 4.6 eV. The semimetallic nature makes graphene as a hole conductor when applied negative voltage while positive gate makes it an electron conductor. Reprinted with permission from Ref. 37. Copyright 2017, John Wiley and Sons. (c)–(e) The current response of graphene FET is varied with the charged target biomolecules on the surface. Reprinted with permission from Ref. 27. Copyright 2019, John Wiley and Sons. (f) A cross-sectional scheme of graphene channel-electrolyte-gate electrode interface capacitance. The electric double layer is about 1 nm in thickness. The equivalent circuit is shown on the left side of the scheme. (g) The geometrical capacitance, quantum capacitance, double layer capacitance of graphene as a function of the number of graphene layers. Reprinted with permission from Ref. 38. Copyright 2013, Nature Publishing Group.

gate voltage, graphene exhibits ambipolar transfer characteristics. This realized the control of type and density of charge carriers with a manipulating of graphene Fermi level (Fig. 1b). When the Fermi level coincides with the charge neutral point, graphene has zero charge carrier density and minimum electrical conductivity.[13] This gate voltage is called the Dirac point voltage (V_{Dirac}) of the graphene device. Because of its semi-metal nature, graphene behaves as an electron-conductor at the positive gate voltage of V_{Dirac} and acts as a hole-conductor at a negative gate voltage of V_{Dirac}.

For Ion-sensitive FET based GFET biosensors, conductivity is tuned with the binding of charged ions or biomolecules due to gate effects.[39] For instance, the V_{Dirac} of the device will move to the high voltage and the conductance will go up with an increase of positive ions concentration. The operation of GFET biosensors is always with the well-defined V_{ds} and V_g, which are the voltage between drain and source and the one between gate and source, respectively. The applied V_{ds} drives charge carriers pass through the graphene channel and it is simultaneously modulated by V_g. Assuming the contacts between channel and source/drain are ideal, which means that there is no voltage drop at both contact points, the current in the lateral direction can be expressed as following:

$$I_{ds} = \frac{W}{L}\mu C_i |V_g - V_{Dirac}|\, V_{ds} \quad [1]$$

Where, W and L are the width and length of the graphene channel, respectively; μ is the charge carrier mobility and C_i is the total gating capacitance of device. The change of μ is a straightforward consequence of molecule adsorption on graphene due to the gating effects. In the case of chemical bond formation between biomolecules and graphene, new scattering centers will be introduced which can rather severely deteriorate its mobility. Hence, channel current I_{ds} is inversely proportional to the total strength of interaction between adsorbed molecule with graphene through the change of V_{Dirac} and the carrier mobility as shown in Figs. 1c, 1d, and 1e.

The applying of gate voltage will lead to the accumulation of ions onto graphene instantaneously. Figure 1f shows the modeling equivalent circuit which represents the interface of the graphene-electrolyte-gate electrode. It is composed of the double layer capacitances (C_L), graphene's quantum capacitance (C_Q), and resistance of the electrolyte in series. The experimentally measured total capacitance C_i is given by:

$$\frac{1}{C_i} = \frac{1}{C_L} + \frac{1}{C_Q} \quad [2]$$

where, C_L is about several tens of μF per cm^2, which is formed at the electrolyte-channel interface by the applied bias voltage;[40] C_Q is determined by the density of states $D(E_F)$ at the Fermi level and can be expressed as $C_Q = e^2D(E_F)$. It has a minimum at Dirac point and displays a continuous increase with V_g moving away from the V_{Dirac}.[41] The systematical studies of the total capacitance between graphene and ionic liquid demonstrate that C_Q dominates the total capacitance when the number of graphene layers is less than four[38] as shown in Fig. 1g (C_g is the geometrical capacitance). Graphene channel has a very efficient gating effect through the liquid-gated configuration. Since the total gate capacitance C_i is approximately 2–3 orders of magnitude larger than a typical back gated capacitance (100 nm SiO_2 is about 345 nF cm^{-2})[19] which makes the gating voltage of a GFET usually less than 1V.

Non-polarizable Ag/AgCl reference electrodes are commonly used as top-gate electrodes (Fig. 1a) to minimize the potential drop at the gate–electrolyte interfaceand obtain artifact-free measurements.[42,43] Another designable configuration is the use of metal electrodes as the top-gate electrode or side-gate electrode (Fig. 1f). In particular, the bio-recognition process that occurs on the functional metal gate electrode will lead to the change of gate voltage, which makes the graphene channel merely works as a transducer.[44] For effective gating, the capacitance of the gate electrode must be an order higher than that of the channel.[45] Otherwise, too much applied gate voltage will drop at the gate-electrolyte interface instead of gating the channel.

Biosensing with GFETs is usually achieved by taking advantage of static or dynamic transfer measurements, which are obtained by examining I_{ds} as a function of V_g (Fig. 2a) either static or time dependent. Bio-recognition procedure can be characterized by measuring the shift of the V_{Dirac}. The dynamic transfer properties characterization is to measure a series of I_{ds} as a function of time at a given gate voltage V_g (Fig. 2b), which reflects the evolution of transfer properties at different stage of reactions. As a crucial parameter, transconductance is defined as the ratio of I_{ds} to V_g:

$$G_m = \frac{\Delta I_{ds}}{\Delta V_g} = \frac{W}{L}\mu C_i V_{ds} \quad [3]$$

A large G_m provokes a large conductance change with charge excitation. For comparison, a typical Si transistor based biosensor has a transconductance around 20 μS for $V_{ds} = 0.5$ V.[47] While for an electrolyte-gated GFET, the value is up to 400 μS with a drain-source voltage in 0.1 V,[48] which is one order of magnitude higher than that of a Si transistor. Generally, the GFETs are operated at their maximum transconductance, with the normalized I_{ds} at V_{ds} and V_g showing the largest change in the transistor current modulated by a small change in the gate voltage. For in-situ monitoring, GFETs are usually integrated with microfluidic devices (Fig. 2c).[46]

Overall, the GFET biosensor works through transducing the resulting perturbation of target molecule adsorption on graphene channel to the change of its conductance. The quality of graphene, substrate choice, metal electrode, functionalization, and the final encapsulation for liquid handling are determining factors to the performance of the sensor. They all will be discussed in the following sections.

Graphene as a high-performance channel material.—As an essential part of GFETs, the properties of graphene play a decisive role in the performance of GFETs. According to Eq. 1, the channel current I_{ds} is proportional to the carrier mobility of graphene. High mobility results in an intense current as well as large transconductance according to Eq. 3 and it is also beneficial for gaining low electrical noise.[4] Many experimental results have shown that

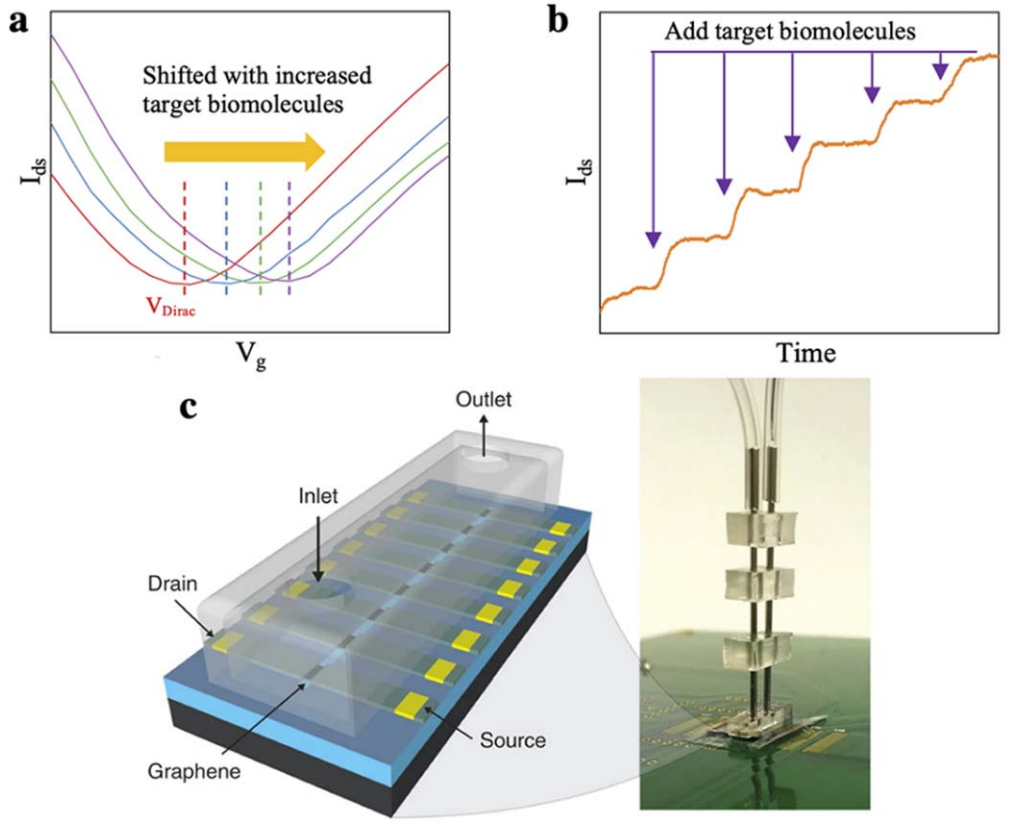

Figure 2. (a), (b) Typical GFET biosensing characteristics plots of I_{ds} vs V_g and I_{ds} vs the time, respectively. (c) Schematic and photograph of an 8-graphene-electrode array with a microfluidic channel configuration on top. Reprinted with permission from Ref. 46. Copyright 2014, Nature Publishing Group.

exfoliated graphene has a much higher detection limit compared with chemical vapor deposition (CVD) graphene and rGO[4] due to its superior mobility.[49] As an essential prerequisite for better understanding the performance of GFET based biosensors, fundamental facts about graphene synthesis, and physical-chemical properties will be briefly discussed first.

Synthesis of single-crystal graphene films.—The most commonly used approaches for preparing high quality graphene are mechanical exfoliation, thermal decomposition of silicon carbide (SiC), and the CVD growth method. The yielded graphene are called exfoliated graphene, epi-graphene and CVD graphene[50] accordingly. The exfoliation method is the initial and mostly applied one in the laboratory. It is to peel off graphene flakes out of highly oriented pyrolytic graphite (HOPG) by Scotch tape. Exfoliated graphene is pristine and normally exhibits very high quality with carrier mobility up to 15 000 $cm^2\ V^{-1}\ s^{-1}$ after transfer and measured on SiO_2/Si wafers at room temperature[51] and the reported highest mobility is 200 000 $cm^2\ V^{-1}\ s^{-1}$ when it was sandwiched by two layers of hexagonal boron nitride (h-BN).[52] However, the lack of scalability severely restricts the scope of its practical applications.

Epitaxial growth on SiC is the method to sublime silicon atoms from hot SiC, leaving behind carbon atoms and reforming a graphene layer on the surface. It is capable of synthesizing single crystalline graphene layers in wafer-scale, and obviate the tedious transfer processes for following electronic device fabrication benefiting from the fact of graphene directly growing on an insulating substrate.[53] The mobility depends on whether the graphene is grown on the silicon face or the carbon face of SiC. Mobility can reach up to and exceed $10^6\ cm^2\ V^{-1}\ s^{-1}$ in the neutral rotated C-face,[54] and it is limited up to 1500 $cm^2\ V^{-1}\ s^{-1}$ on the Si-face.[55] Epitaxial graphene on the silicon face is capable of growing monocrystals and is well-controlled as single-layer or bilayer because of the self-limiting sublimation. The investigation via Raman spectroscopy indicates the existence of unignorable interaction between epitaxial graphene and substrate.[56] Epi-graphene transferred on SiO_2/Si substrate exhibits increased mobility [57] up to 2700 $cm^2\ V^{-1}\ s^{-1}$. Besides, hydrogen intercalation of buffer layer resulted in quasi-free-standing epitaxial graphene layer also demonstrates improved carrier mobility[58] to 2000 $cm^2\ V^{-1}\ s^{-1}$. Epitaxial graphene has great potential in the electronic device industry and the production costs dropped dramatically in recent years.

In contrast to the thermal decomposition of SiC in which the substrate itself is the carbon resource for graphene growth, in the CVD method, an extra gaseous carbon source is needed, and a metallic substrate is usually required severing as both catalyst and substrate to grow the graphene.[59,60] Besides, in order to fabricate GFET based biosensor, one crucial transfer step must be conducted, which is necessary for dissolving the metallic substrate. So far, the measured mobility of CVD grown graphene is in the range of 1 000–70 000 $cm^2\ V^{-1}\ s^{-1}$ [61] and even higher values have been reported by encapsulation in h-BN.[62,63] Due to its simple fabrication procedure and rather high quality, it is very suitable for low cost laboratory research, most of the reported GFET biosensors are CVD-grown graphene so far.[27] The method of roll-to-roll transferring CVD graphene has attracted attentions in terms of excellent mechanical properties, electrical properties, and compatibility with flexible substrates.[64] It also benefits in high production efficiency and cost effective production. However, in order to achieve scalable production of GFET biosensor, the transfer of graphene to the target substrate is still a thorny issue, especially to silicon wafer substrates.[65] The uncontrollable defects and contamination introduced during the transfer process caused a great fluctuation in the performance of the sensor devices. From this perspective, the

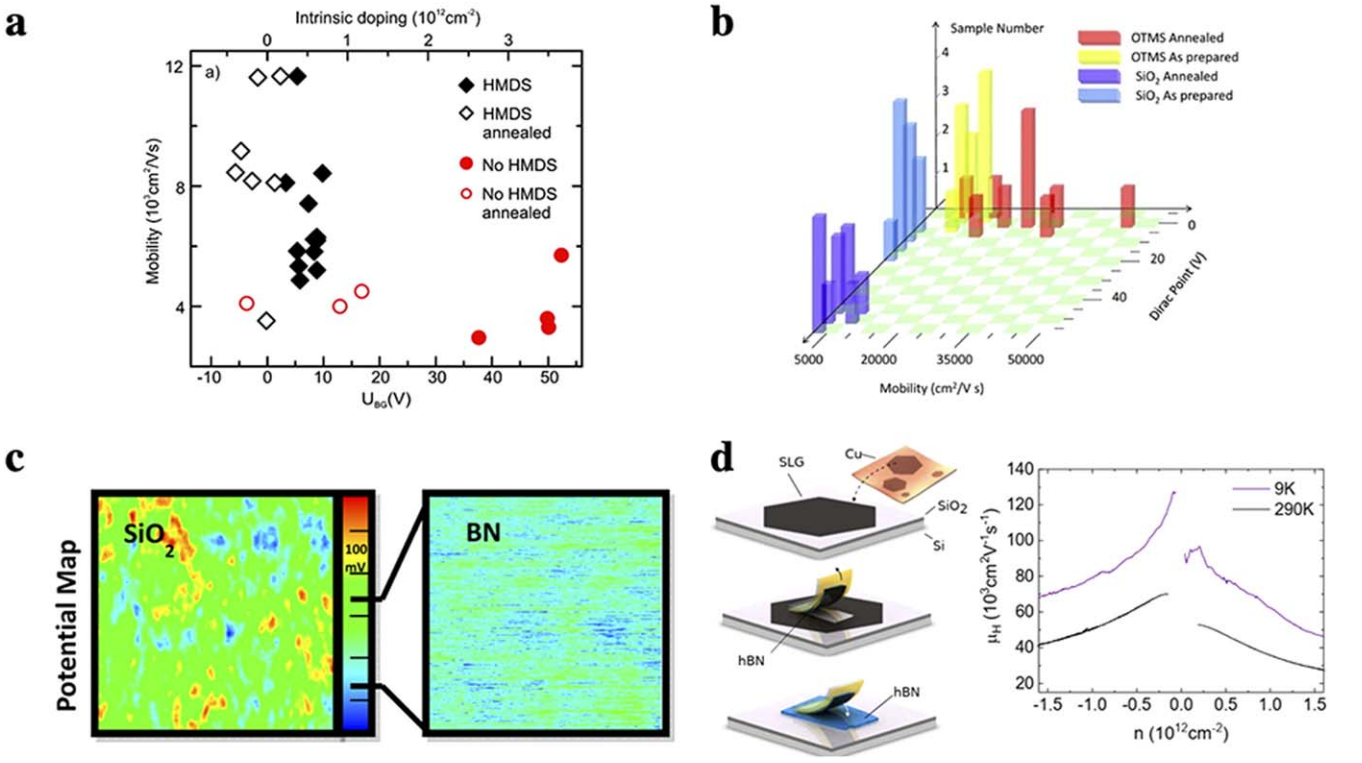

Figure 3. (a) Mobility and Dirac point of different graphene transfer to SiO_2 substrate with or without HDMS. The annealing process in vacuum at 140 °C for 1 h resulting in a shift in a shift of the Dirac Point to near-zero gate voltage. Reprinted with permission from Ref. 71. Copyright 2010, American Chemical Society. (b) Histogram of mobility and the Dirac point of different graphene on bare SiO_2 substrate and on OTMS-modified SiO_2 substrate. The annealing process has a restoring effect of the high electrical conductance and Dirac point of the graphene. Reprinted with permission from Ref. 72. Copyright 2011, John Wiley and Sons. (c) The Kelvin probe microscopy image of the local electrostatic potential fluctuations on h-BN substrate and bare SiO_2 substrate. Reprinted with permission from Ref. 67. Copyright 2011, American Chemical Society. (d) Schematics of encapsulate graphene in h-BN through a wet transfer process. Density-dependent graphene mobility at 9 k and room temperature. Reprinted with permission from Ref. 74. Copyright 2019, American Chemical Society.

epitaxial growth method of directly synthesizing high-quality monocrystal graphene on an insulating substrate is another ideal candidate for the pursuit of a reliable and reproducible manufacturability electronic device.

Substrate tunable properties.—Since graphene is only a single atomic layer, it is strongly influenced by the underlying substrate.[61] In terms of applications for GFET biosensors, we should not only concern about the electronic transport influence of the substrate but also need to match the sensing functional requirements. Although SiO_2/Si wafer is a commonly selected target substrate for 2D material transfer, it has drawbacks including relatively rough surface, impurities, and charge puddles introduced by electron beam exposure.[66,67] These will lead to scattering and inhomogeneities of charge carrier inside the supported graphene and further result in the degradation of its electric conductivity. The annealing process in a vacuum environment will effectively remove the charge puddles and greatly reduce the unsaturated chemical bonds at the dielectric surface, which as a result will increase the performance of GFET devices.[68] However, the primary source of substrate for GFETs remains SiO_2/Si despite their carrier mobility being less than ideal.

Suspending graphene channel over a gap of the dielectric substrate could avoid impurity and phonon scattering. This could improve the carrier mobilities,[69] but it is not suitable for practical biosensor configuration. A feasible way to screen the scattering effects is to add a shielding layer between the dielectric and graphene by self-assembled monolayer (SAM) or h-BN.[68] GFET on SAM-covered SiO_2/Si substrates demonstrated improved mobility by attenuating surface polar phonon scattering and suppressed hysteresis caused by reduced charge inhomogeneity.[70] Hexamethyldisilazane (HMDS)[71] and octadecyltrimethoxysilane (OTMS)[72] are typically used molecules for SAM shield layer. As shown in Figs. 3a (HMDS), 3b (OMTS), by shielding with SAM as the substrate, the mobility increases and the intrinsic doping level is lowered. Monoclonal antibodies functionalized CVD graphene on HMDS coated substrate achieves 0.01 fM detection capability of the cancer biomarker CSPG4, which is five orders of magnitude better than that by a conventional colorimetric assay.[73]

h-BN has been regarded as an ideal dielectric substrate for improving the performance of graphene-based devices. h-BN has a similar lattice structure to graphene, hence is also called "white graphene",[75] but, it has a completely different electronic structure with a large bandgap of 5.97 eV.[76] It has an atomically smooth surface almost free of dangling bonds and charge traps. As shown in Fig. 3c, the high vacuum Kelvin probe microscopy measurement demonstrates 1–2 orders of lower potential fluctuations of h-BN than SiO_2, which largely diminishes the deterioration of graphene mobility due to the so called substrate effect.[67] Through conventional wet transfer method (Fig. 3d), the highest reported mobility of exfoliated h-BN supported single-layer CVD graphene is 70 000 cm^2 V^{-1} s^{-1} at room temperature.[74] The recently developed wafer-scale, single-crystal h-BN growth on Cu (111) thin films could open much broad scope of deeply exploiting the extremely high mobility of pristine graphene.[77]

Recently, graphene also has extensive applications in flexible electronic due to its mechanical properties and optical transparency.[37,78–80] Polyethylene terephthalate (PET), polydimethylsiloxane (PDMS), polymethylmethacrylate (PMMA), and Polystyrene (PS) are commonly selected flexible substrates.[81,82] As one of the most widely used flexible substrates, PMMA severely degrades the mobility of its supported graphene, with the reported values similar to those of graphene on SiO_2 support.[83,84] The PMMA residues left on the graphene surface result in chemically active contamination and n-type doping.[85] Spectroscopic studies revealed that oxygen-containing functional groups react with electrophiles or nucleophiles that cause graphene mobility degradation.[86] Therefore, cleaning graphene transferred to flexible substrates such as PDMS,[85] polyolefin,[86] polyethylene Polyethylene naphthalate (PEN)[87] and paraffin[88] exhibit an improvement in graphene transfer mobility. The strategy of the shielding layer between the dielectric layer is also applicable to the flexible substrate. Luca et al. have picked up CVD-grown graphene from copper foil catalyzers through a polymer stack (consisting of PVA and PMMA) covered with h-BN flake on a PDMS stamp substrate. The graphene encapsulated with h-BN on PDMS substrate demonstrated outstanding mobility of 50 000 cm^2 V^{-1} s^{-1} at room temperature.[62] These exploratory works prove that graphene has great potential in flexible electronics. The use of flexible substrates can realize sensing applications such as wearable and skin implanted in-vivo measurements, which will greatly enhance the applicable range of GFET biosensors. For example, some flexible GFET devices have been used to achieve real-time monitoring of cortisol stress hormone[89] and implantable brain mapping.[90]

Defects engineering.—Anything that breaks the initial symmetry of the infinite carbon honeycomb lattice will induce defects.[91,92] Defects can be introduced during graphene synthesis, processing, and applications. They can be edges, grain boundaries, vacancies, wrinkles, doped atoms, hybridization of carbon atoms from sp^2 to sp^3, electronic interactions with the nanoparticles or polymer residues[93–97] and even the interactions with substrate or external field can be viewed and treated as defects. Defects in the channel of GFET will largely change its sensing responses.[98] This will also lead to a doping effect or to charge transfer due to the interaction of the graphene-electrolyte interface. Fu et al. demonstrated that defect-less graphene exhibited weak pH sensitivity. Graphene passivated with the inert aromatic molecule fluorobenzene suppressed sensitivity to solutions' pH values as shown in Fig. 4a. In contrast, the defective graphene is much sensitive to the variation of pH values, which caused an obviously Dirac point shift (Fig. 4b).[21] In some cases, unsaturated dangling bonds caused by vacancy defects present in the graphene could direct wiring with undesirable biomolecules that possibly deteriorate the repeatability of the sensor.[99,100]

In contrast to high-performance graphene-based electronics pursued short channel and high carrier density,[18] extra defects modulation to enhance biological detection is necessary for GFET based biosensors.[97] RGO based FET sensors displayed much better sensing response as a result of a large concentration of defects compared to near defect-free exfoliated graphene.[106,107] However, gaining this high sensitivity is at the cost of degradation in the mobility and quite a high noisy level of the signal. It is essential to reach the balance between amount of defects and maintaining a certain level of electrical transport performance. For instance, Wu et al. demonstrated that the sensitivity of graphene to dopamine and serotonin is highly dependent on point defects.[108] Its sensitivity increases with the density of point defects, but once it reaches an optimal value, introducing more point defects will reversely lead to the sensitivity decrease. Very recently reported nano-engineered graphene electrode with an optimized density of point defects exhibits up to 20 times higher sensitivity than the conventional carbon-based electrode. Therefore, appropriate control of the introduced defects is essential for realizing high performance GFET biosensors.

Electrochemistry of graphene.—Generally, GFET biosensing is most directly operated in an electrolyte solution. In such a configuration, the graphene channel is in contact with the electrolyte interface and is coupled with an electrolyte-gate voltage. The electrochemical reference electrode such as Ag/AgCl represents a common choice of gate electrode owing to their ultrastable solution potential. Therefore, the electrochemical properties of graphene are merit deep study and discussion, because it will have an interplay with in-plane transport. Ideally, the crystal lattice of graphene is free of dangling bonds and is electrochemically inert. Due to the existence of defects, even a tiny electrochemical current (or gate leakage current) generated by the redox reaction causing by either charge transfer with ionic or possible redox species will flow vertically through the graphene channel and add to the output

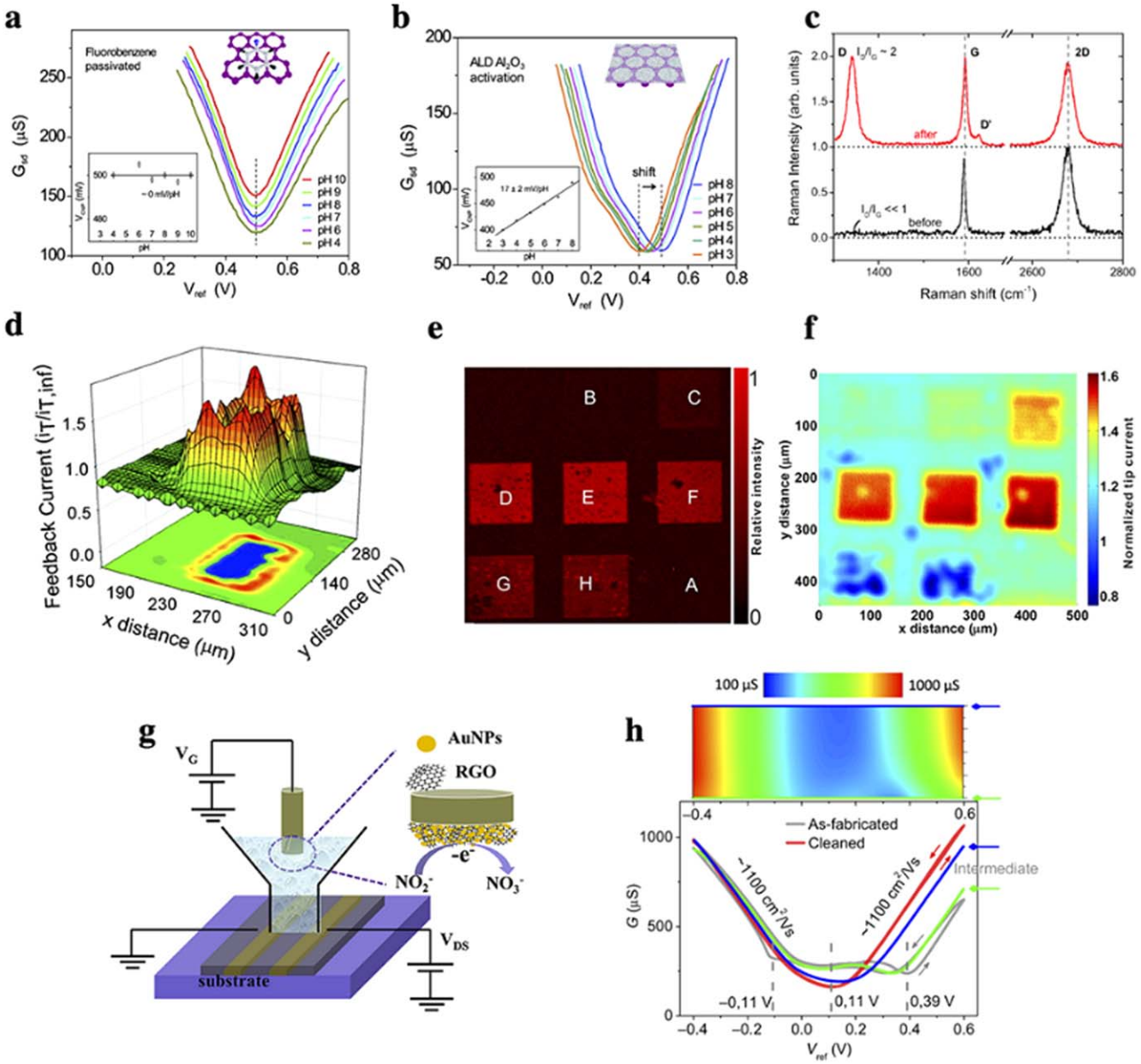

Figure 4. (a), (b) The conductance of source and drain vs gate potential V_{ref} of fluorobenzene functionalized and Al_2O_3 coated GFET device in different pH buffer solutions, respectively. Inset: the sensitivity of GFET to pH values. Reprinted with permission from Ref. 21. Copyright 2011, American Chemical Society. (c) The Raman spectra of the graphene before gate potential were applied and after the electrochemical reaction occurred. A distinct D peak has emerged after the electrochemical reaction. Reprinted with permission from Ref. 101. Copyright 2015, American Physical Society. (d) SECM images of graphene with a mechanically induced defect on SiO_2 substrate. Reprinted with permission from Ref. 102. Copyright 2012, American Chemical Society. (e) Raman mapping of defective graphene patterns with various defect densities induced by irradiation. (f) SECM images of the same defective graphene patterns. The tip potential is 0.4 V and the substrate potential is 0.11 V. Reprinted with permission from Ref. 103. Copyright 2014, American Chemical Society. (g) Schematics of GFET nitrate sensor. The changes of gate voltages applied to the graphene channel are induced by electrooxidation of nitrite at gate electrodes. Reprinted with permission from Ref. 104. Copyright 2019, Elsevier. (h) The upper panel shows the conductance of GFET during electrochemical cleaning cycles in an operation range from −0.4 V to 0.6 V. Lower panel shows the conductance of GFET vs gate potential V_{ref} before electrochemical cleaning (gray line), with the first electrochemical cycle (green line), after 5 electrochemical cycles (blue line), and after 10 electrochemical cycles (red line). After 10 electrochemical cycles cleaning process, the GFET demonstrated a rather symmetric ambipolar behaviour with carrier mobility of 1100 $cm^2\ V^{-1}\ s^{-1}$. Reprinted with permission from Ref. 105. Copyright 2017, the American Association for the Advancement of Science.

current. When gate voltage exceeds the threshold, more than 1 nA leakage current will occurs, consequently will introduce more defects, which has been confirmed by Raman investigation as shown in (Fig. 4c).[101,109] In order to suppress the influence of this electrochemical reaction process on the detection current, GFET biosensor generally works at a lower gate voltage.

The electrochemical properties of graphene have been extensively studied.[110–113] It demonstrates similar behavior in many ways to graphite.[114] Single-layer pristine graphene has a slow heterogeneous electron transfer (HET) rate towards the redox probes that are mainly due to its geometric feature of small edge plane and large basal plane. More detailed electrochemical characters were revealed through both inner-sphere and outer-sphere redox probing, in which the inner-sphere redox mediator is determined by the surface and the outer-sphere highly depends on the density of states (DOS) of the bulk.[115,116] Studies on the electrochemistry of potassium

ferricyanide $K_3Fe(CN)_6$ (inner-sphere redox couple) on single-layer graphene containing defects demonstrated that the standard heterogeneous rate of electron transfer (k^0) at the structural defect sites was about 1 order of magnitude higher than the basal plane and more reactive than the overall surface of graphene.[102] Aleix et al. demonstrated that for $Ru(NH_3)_6^{3+/2+}$ (outer-sphere redox couple), there was a strong dependence of k^0 on the layer number of graphene, with monolayer having the slowest rate.[113] Overall, the edge planes dominate the electrochemical response of graphene. More evidences came from the investigations through combining Raman spectroscopy with SECM, which quantified the correlation between density of defects and localized electrochemical activity of graphene (Figs. 4e, 4f).[103]

The same as the GFET biosensor, the graphene biosensor based on the electrochemical detection also uses the graphene surface as the main sensing element.[4] Different from the change in graphene conductance caused by gating voltage, the sensing principle of graphene electrochemical biosensor roots on the electrochemical transfer current between the redox active biomolecules in the electrolyte and graphene surface.[117] The fast electron transfer and excellent electrocatalytic capability of graphene enable effective detection of the target biomolecule during the redox process, which demonstrated a improved selectivity.[118] Recently, more researchers start to focus on exploiting the electrochemical properties of graphene to improve the performance of GFET biosensors. A transistor constructed by combining Au nanoparticles modified rGO on the gate electrode with a monolayer graphene channel reaches a very low detection limit of nitrite (Fig. 4g).[104] Its excellent sensing capability is attributed to the electrochemical oxidation of nitrite induced changes in effective gate voltages. In addition to achieving electrochemical charge transfer for the potential drop, electrochemical reactions are also used in treating graphene surface. Fenoy et al. completed electrosynthesis of an amino moiety-bearing polymer layer on the graphene channel via voltammetry.[119] A copolymer poly (3-amino-benzylamine-co-aniline) (PABA) provides a suitable electrostatic charge and non-denaturing environment for enzyme immobilization, and it also improves the pH sensitivity of the sensor. Fu et al. also used an in situ electrochemical method to rapidly clean the graphene surface, removing contaminants and improving the performance of GFETs (Fig. 4h).[105] The development of this kind of hybrid technology is expected to further enhance the selectivity and functionality of GFET biosensors.

Device fabrication.—In this section, the structure of GFET biosensors will be discussed, which involves issues about FET configurations, metal contacts, and Debye screening.

FET configurations.—As previously discussed, the working principle of the GFET biosensor is realized by modulating the density and polarity of charge carriers in the graphene by the absorbed target molecules and their gating effects. At least three electrodes are included in the minimum structure of the GFET biosensor. The source and drain electrode make direct contact with the graphene which enables electrical transfer through the channel. According to the differences in shape and position of the gate electrode, there are multiple configurations. The back-gate configuration is usually applied when FET sensors are used in air or other gaseous environments. There, the conductive layer under the substrate is used as the gate which is separated from the graphene and the source-drain electrodes by an insulating layer. It has demonstrated detection capability of single gas molecules.[3,120]

However, in most cases for biomolecule detection, the gate electrode of GFET needs to operate in an electrolyte solution. This configuration is often named "liquid-gate," in which the gate voltage is applied with either a reference electrode immersed in the electrolyte or a side gate electrode patterned on the substrate. Reference electrode made of Ag/AgCl is a conventional choice. As a reference electrode, Ag/AgCl demonstrates superior performance than that of platinum wire, which gives highly accurate measured protein binding process.[43] Inplane metallic gate electrodes are patterned as the source and drain electrode, which allows the fabrication of arrayed GFET electronic devices. Several metals have been used for making inplane gate electrodes, such as platinum,[121] silver[122] and gold.[123–125] In recent years, new kinds of gate materials have been applied in GFET sensors. For example, it has been demonstrated that the graphene transistors gated by bioactive hydrogels could achieve highly specific sensing.[126] There, the microenvironment created by the hydrogel gate exhibits excellent biocompatibility and could maintain the ability of enzyme recognition for at least one week. This new gate configuration shows multiple detection of target molecules in the same graphene-based platform.

Metal electrode contact.—Large contact resistance has always been a bottleneck for realizing high-performance GFET sensors.[127–130] Compared with traditional semiconductor devices, 2D electronics have a very short channel, so the resistance of the channel is greatly reduced and the contact resistance becomes dominant.[68] The poor charge injection and low on-current between graphene and the metal electrode severely limited the performance and power consumption of the GFET device. Typically, the high contact resistance between metal electrodes and the graphene mainly due to the lack of surface bonding sites on each side[131] and strong orbital hybridization.[129,132–138] The contact resistance of metal-graphene is around a few thousand of $\Omega\cdot\mu$m,[128,139] which is about hundred times higher than that of silicon-based electronics.[140]

Great efforts have been dedicated to reduce contact resistance. The primary method is to maximize the Fermi-level difference between the metal and the graphene to enlarge graphene's DOS.[127,132,141] Metals with varying work functions have been explored to form Ohmic contact with graphene. Commonly used metals include Cr/Au and Ti/Au (Fig. 5a). But this method is limited by the difficulty in controlling doping level of the graphene.[139] Application of thermal annealing[142–144] and delicate ozone/ion beam treatment of contacts[145] are also reported. One much significant method is to employ edge-contact instead, where metal electrode contacts graphene laterally along the edges. As shown in Fig. 5b, the reported edge contact resistance of is about 100 $\Omega\cdot\mu$m on an exfoliated monolayer graphene[16] and the sheet resistivity is less than 40 Ω per square at $n > 4 \times 10^{12}$ cm^{-2}, where n is the charge carrier density (Fig. 5c). Later, Smith et al. patterned the source/drain contact regions of graphene and cleaned them with oxygen plasma. This led to a 32% reduction in contact resistance after annealing.[138] Passi et al. performed a systematic investigation to optimize contact configurations with patterns of holes in graphene under an Au electrode and achieved a substantial decrease in contact resistance from 1372 $\Omega\cdot\mu$m to 456 $\Omega\cdot\mu$m.[146] Further improvement was achieved by electrostatically doping graphene, set the lowest contact resistance record of 45 $\Omega\cdot\mu$m, so far.

By using suitable conductive metals and processing with the contact interface, the contact resistance between the graphene and the electrode can be significantly reduced and has good stability. Some of the recent research in this field has improved the applicability of the device. Liu et al. achieved a very low contact resistance of 45 $\Omega\cdot\mu$m through an unintuitive bottom-contact strategy incorporating transfer procedure without any harsh thermal treatment (Fig. 5d).[147] This cost-effective and easily achieved van der Waals (vdW) contact method shed the light on large scale production of future GFETs based flexible biosensors.

Debye screening.—Although GFET biosensor is a promising candidate for single-molecule detection, it is still impeded by fundamental ionic screening in high ionic strength solutions, known as the Debye screening effect.[148] GFET biosensors are sensitive to the binding of charged molecules on the surface due to the consequent electrostatic gating or charge transfer. The charged surface attracts counterions in the electrolytes, forming an electrical double layer and screening off the charged molecules, hereby

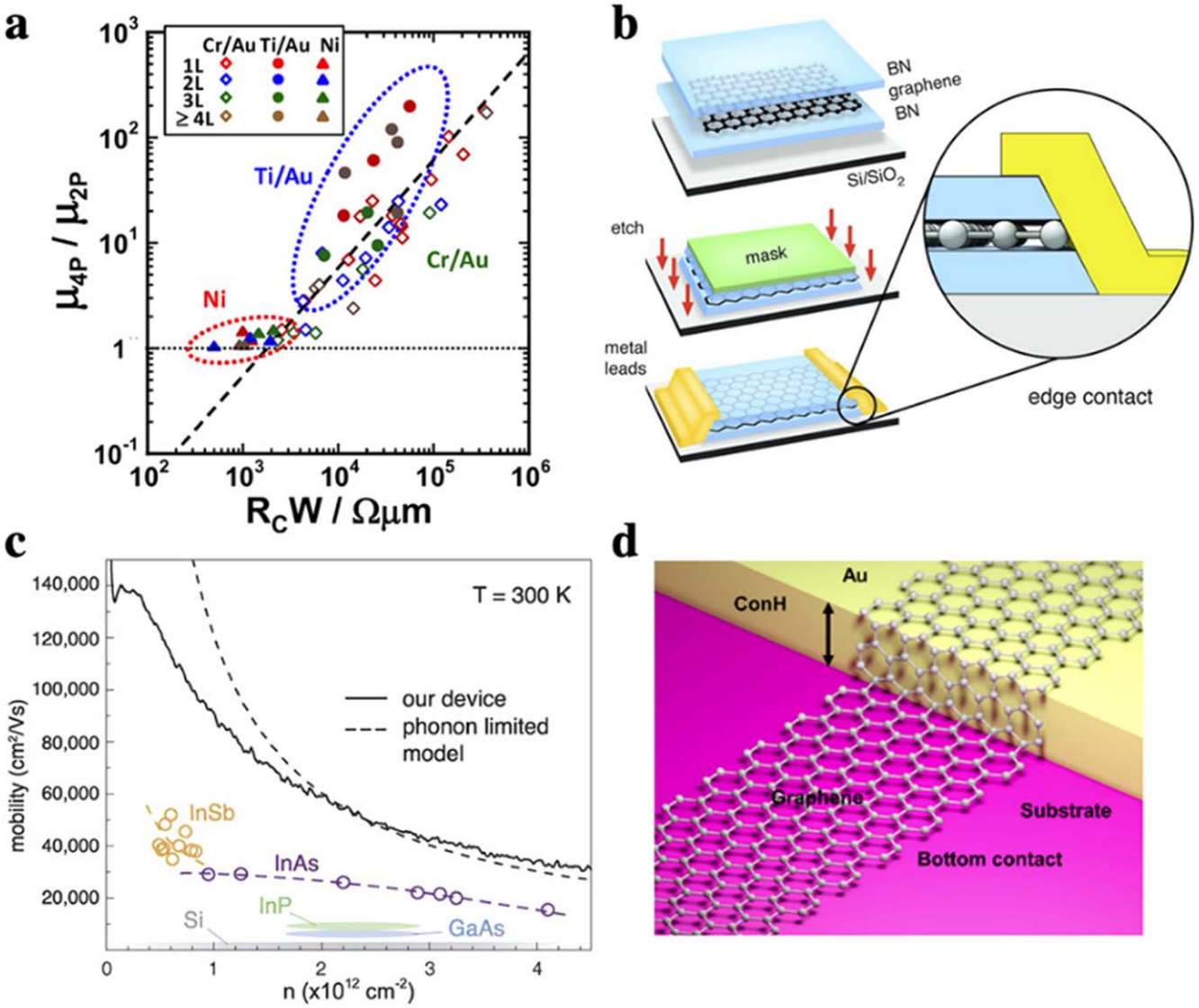

Figure 5. (a) The ratio of 4-probe mobility (μ_{4p}) of 2-probe mobility (μ_{2p}) as a function of contact resistivities (R_CW) for the different contact metals Cr/Au, Ti/Au, and Ni. Reprinted with permission from Ref. 139. Copyright 2017, AIP Publishing. (b) Schematic illustration of fabrication edge contact of graphene encapsulated in h-BN. (c) The mobility of edge contact graphene transistor vs gate potential charge carrier density (n) at room temperature. Reprinted with permission from Ref. 16. Copyright 2013, the American Association for the Advancement of Science. (d) Schematics of graphene-metal vdW contact via bottom-contact strategy. Reprinted with permission from Ref. 147. Copyright 2019, American Chemical Society.

reduces the field produced by analyte on the graphene surface.[148–150] This screening effect depends on the distance between the graphene surface and the target biomolecules, characterized by the Debye screening length $\lambda_D = 0.304/I^{1/2}$, where I is the ionic strength of the electrolyte solution. The electrical signal decays to 36.8% (1/e) of its original value at a one Debye length.[151] Typically, at room temperature in 100 mM buffer solution, λ_D is around 0.7 nm, then, the electrostatic interaction between molecule and graphene will be extremely weak when they distance more than a few nanometers. As shown in Fig. 6a, the larger the molecule, the stronger the screening effect. As a result, desalting to low ionic strength solution was utilized to increase Debye length.[148,151] Sebastian et al. demonstrated that the sensing response of the hybridization of complementary DNA molecules increases from 12% to 80% by decreasing the buffer concentration from 1X PBS to 0.1X PBS.[150] However, the desalting procedure is usually tedious and not suitable for real-time detection. Another traditional approach is to use of short receptors to reduce the distance between the channel surface and the target analyte.[152] In addition, modification of the channel material with a biomolecule-permeable polymer layer also demonstrated an effective increase in the Debye length.[153]

In recent years, many ingenious approaches have been proposed to resolve the Debye screening issue. Ono et al. demonstrated that Debye length interference can be diminished by detecting the enzymatic products instead of directly sensing the target biomolecule through enzymatic reaction. Because the target yields reaction products that can diffuse freely to the graphene surface and it is independent of Debye screening. As an example, urease was reported to be selected to make ammonia, then was detected using GFET sensor (Fig. 6b),[155] consequently as low as 0.04 bacterial cells were successfully detected within 30 min through this indirect sensing method. Also, Hwang et al. present a new method to increase the Debye length by curving the morphology of sensing materials (Fig. 6c).[156] Regarding GFET, computational simulations indicate that "electrical hot spot" will be formed in the channel by simply bending it, which resultantly will reduce the charge screening at the nanoscale deformations regions. This was experimentally demonstrated by a GFET biosensor with a bent channel showing

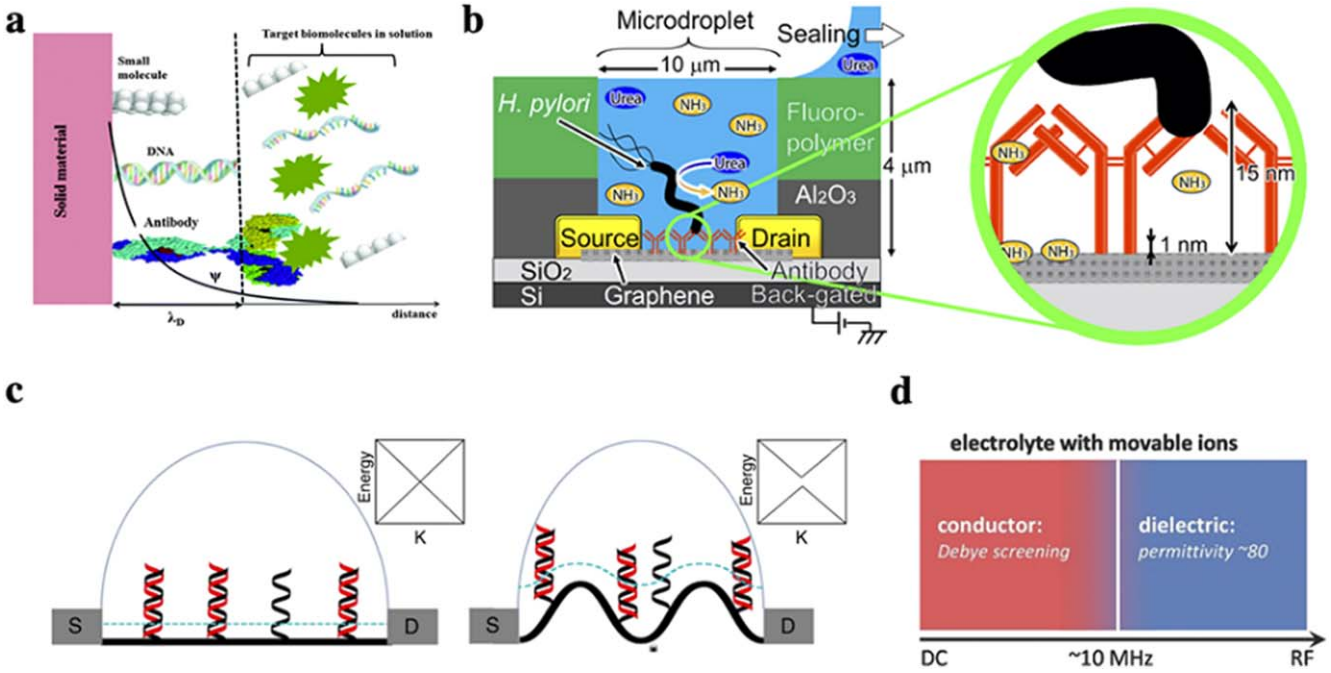

Figure 6. (a) Schematic illustration of the diffuse layer of the electrical double layer and different bio-recognition biomolecules as well as corresponding target biomolecules. Reprinted with permission from Ref. 154. Copyright 2015, Royal Society of Chemistry. (b) Schematics of enzymatic GFET biosensor. The graphene channel is functionalized to capture the target biomolecule (H. pylori). The enzyme urease was selected to generate ammonia, which could directly detect by GFET. Reprinted with permission from Ref. 155. Copyright 2019, American Chemical Society. (c) The cross-sectional scheme of the flat and crumpled GFET biosensor. The Debye length in the ionic solution is increased by the crumpling of graphene (blue dot lines). The inset on the right side represents that the bandgap of graphene may open by the crumpling process. Reprinted with permission from Ref. 156. Copyright 2020, Springer Nature. (d) The electrolyte has the Debye effect under low-frequency voltage lower than 10 MHz and demonstrated as dielectrics at high frequencies. Reprinted with permission from Ref. 4. Copyright 2017, John Wiley and Sons.

detection of DNA/RNA molecules down to 600 zepto-molar (zM) of the LOD.

High frequency detection is another option to overcome the Debye screening effect (Fig. 6d).[27] The movement of the charged solvent dipoles will lag behind the change of the AC electric field, which is frequency dependent.[157] Therefore, liquid solutions behavior as dielectrics at high frequencies and could diminish the Debye screening. However, since high frequency signals can deeply diffuse into the buffer solution, it will introduce much external environmental noise.[27]

For electrolyte-gated GFET biosensing, the charge screening by ions in various medium needs to be considered and modeled by the Debye length. Many strategies have been proposed for overcoming this issue while maintaining physiological environmental conditions. The application of these strategies can greatly enhance the detection range and scalability of the GFET sensor.

Graphene Functionalization for Biochemical Sensing

In most cases, the large aromatic sp^2 carbon lattice of graphene possesses only a few dangling bonds and is chemically inert to molecules under ambient conditions. The unsaturated carbon bonds can only transfer electron with very few molecules, such as dopamine, ascorbic acid, and DNAs, but without selectivity. Functionalization of graphene could largely expand the sensing scope of target biomolecules including proteins, bacteria, DNAs, odorants, and viruses.[12,24,25,158] The conventional strategy is to build up an bio-recognition layer through either covalent bonding or non-covalent interactions, which is consist of nucleic acid, enzyme, and nanoparticles, etc.[159] Particularly, we will discuss nanoparticle functionalizing graphene that offers extra unconventional physico-chemical properties which largely extend application scope of GFET biosensing. More comprehensive and detailed reviews of the functionalization of graphene can be found in Refs. 22 and 160.

Covalent functionalization.—The so-called covalent functionalization of graphene is to establish covalent linkages between functional groups and graphene through the π bonds. It occurs by converting sp^2 to sp^3 hybridization, which requires the involvement of high energy reactants such as strong acids or radicals.[160] This transformation also creates a geometric distortion that extends to multiple lattices and may results in the gap opening of graphene band structure.[161–163] A typical example is that graphene opens a 2.93 eV bandgap after 25% coverage of fluorination.[164] Covalent functionalization has a strong interaction with the honeycomb lattice through forming covalent bonds. The commonly used functional groups include organic free radicals (aryl diazonium), oxygen functional groups (carboxyl, hydroxyl, and epoxy moieties), heteroatom atomic species (H, F, and O). Additionally, the hydrophobic nature of graphene is modified after covalent functionalized with hydrophilic groups grafted onto its basal plane.[165]

In terms of GFET biosensing applications, one of graphene covalent functionalization is to introduce oxygen-containing functional groups such as carboxyl and epoxide groups. Islam et al. developed a smart GFET biosensor for the detection of the human immunodeficiency virus (HIV) and its related diseases: cardiovascular disorders (CVDs) and rheumatoid arthritis (RA)[166] by taking the advantage of the fact that many amino groups contained biomolecule could form stable amide bonds with carboxyl groups under the assistance of EDC/NHS (1-Ethyl-3-(3-dimethylaminopropyl) carbodiimide hydrochloride (EDC) and N-hydroxysuccinimide (NHS)). The antibodies were covalently conjugated to exfoliated graphene via EDC and NHS carbodiimide activation (Fig. 7a). The Raman spectra demonstrated a shifted and weakened 2D peak, as well as an increased D peak induced by antibody binding. The LOD was 100 fg ml^{-1} for HIV biomarkers and 10 fg ml^{-1} for CVDs and RA biomarkers under standard optimized conditions. Tehrani et al. developed diazonium functionalized epitaxial graphene as the channel of GFET for cancer risk biomarker

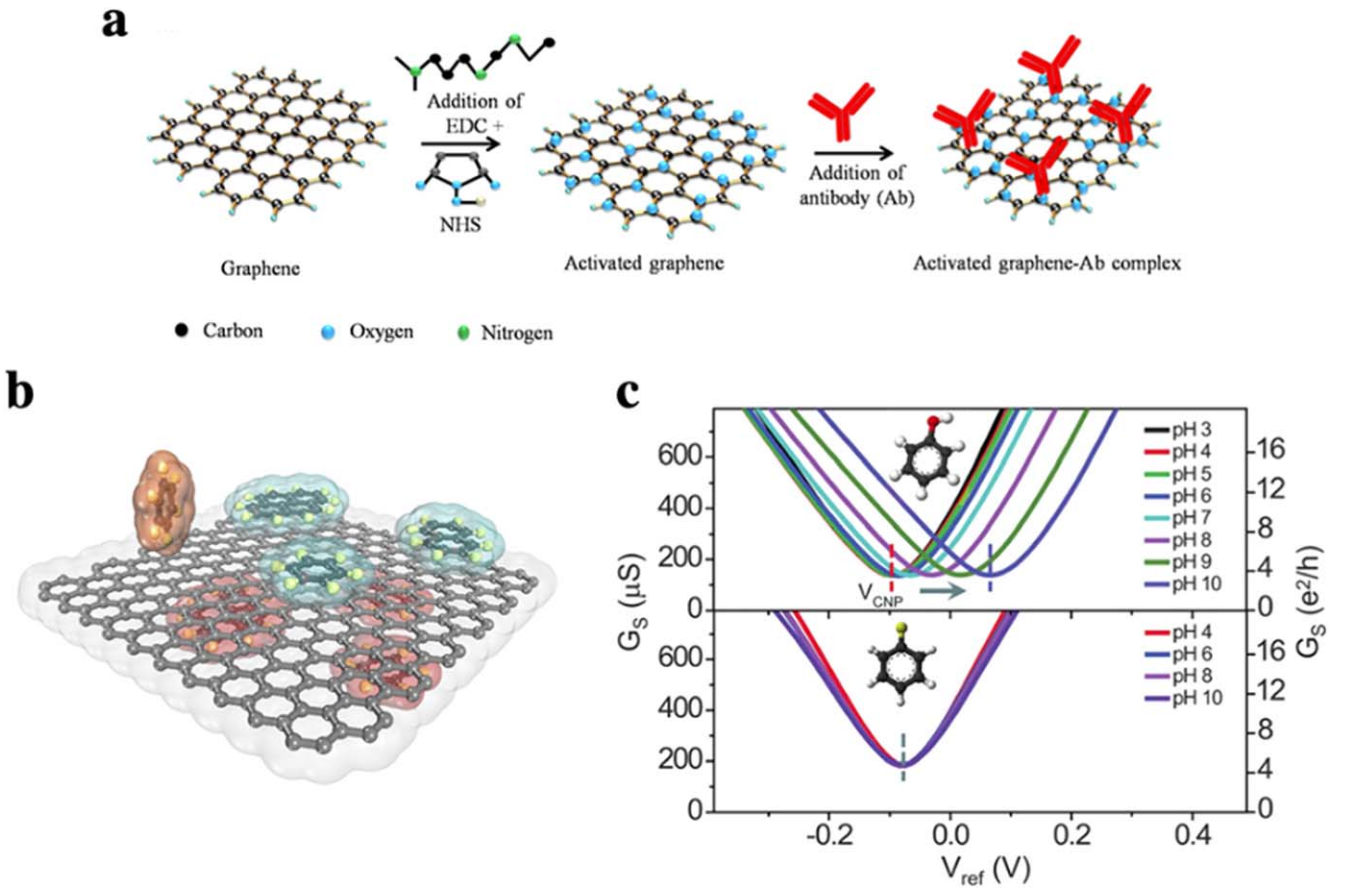

Figure 7. (a) The procedure of covalently conjugated antibody to graphene surface by using EDC and NHS carbodiimide activation. Reprinted with permission from Ref. 166. Copyright 2019, Elsevier. (b) Schematics of noncovalent functionalization of graphene with idealized π–π or C–H·π interactions. Reprinted with permission from Ref. 170. Copyright 2016, American Chemical Society. (c) The conductance of GFET device vs reference potential V_{ref} in different pH buffer solutions. The phenol functionalized graphene demonstrated an enhanced pH sensitivity. In contrast, fluorobenzene functionalized graphene passivate the pH sensitivity. Reprinted with permission from Ref. 171. Copyright 2013, Royal Society of Chemistry.

8-hydroxydeoxyguanosine (8-OHDG) detection, which reaches an excellent detection limit of 0.35 nM.[167] However, covalent functionalization sacrifices the sp^2 structure of graphene, therefore severely decreases its charge carrier mobility.[168,169] From this perspective, many non-covalent functionalization approaches which less perturbation of the π conjugated structure have been developed recently.

Non-covalent functionalization.—Non-covalent functionalization is mainly based on vdW force or $\pi-\pi$ interaction, which introduces new chemical groups or molecules to graphene surface.[159] Many studies also have found that non-covalently functionalized graphene can retain its high mobility.[172] This is particularly important for fast sensing. Higher mobility implies a fast-current response, as was pointed out in Sections 2.1. Thus, non-covalent functionalization is very appealing for realizing high-performance GFET biosensors. Graphene has a large extended aromatic surface with almost planar geometry, which prefers to have $\pi-\pi$ interactions with small aromatic molecules. The $\pi-\pi$ interaction occurs between the electron-rich and electron-deficient part that exhibit face-to-face and edge-to-face arrangement[170] as represented in Fig. 7b. For instance, naphthalene,[173] anthracene,[174] pyrene,[175] pyridine,[176] fluorinated benzene derivatives,[177] DNA,[178] proteins,[179] and peptides[180] have been decorated on graphene. Fu et al. non-covalently functionalized graphene with aromatic molecules containing OH groups (phenol),[171] which effectively preserves mobility of graphene also exhibits an enhanced pH sensitivity (Fig. 7c).

As one of the most frequently used molecules in graphene functionalization, 1-pyrenebutanoic acid succinimidyl ester (PBASE) is chosen as a linker to assist anchoring of biomolecule.[181] The aromatic pyrenyl group π-stacks with the surface while the succinimidyl ester group specifically reacts with amine terminal groups of the biorecognition molecule to form an amide bond.[182] Up to now, many types of biomolecules have been successfully anchored to graphene through PBASE linkers such as peptides, antibodies, enzymes, and avidin, as well as DNA probes (Fig. 8a), and displays very good electrical performance (Figs. 8b, 8c and 8d).

The controversial issue of non-covalent functionalization is its relatively weak interaction, which will affect the stability of the sensor. The strength of non-covalent interaction is on the order of 0.1–100 kJ mol^{-1} and most are less than 20 kJ mol^{-1}, which is about 2–3 orders of magnitude smaller than that of ionic or covalent bonds (about 100–1 000 kJ mol^{-1}).[184] Although the energy of individual non-covalent interaction is lower than a covalent bond, it is still large enough to support the bioreceptor to realize wearable sensors and substrate based biosensors.[185,186] Wang and colleagues demonstrated a flexible and stretchable GFET biosensor with high selectivity and low LOD to an inflammatory cytokine biomarker (TNF-α).[187] PBASE was used as the linker to immobilize the bioreceptor (single-stranded DNA VR11) on the surface through non-covalently π–π stacking. It shows highly constant sensitivity with a variation less than 2%.

Functionalize with nanoparticles.—Noble metal nanoparticles (NPs) and NPs-modified electrodes are widely used in catalytic and electro-optics.[23,188] Many works have demonstrated NPs' sizes, shapes, spatial distribution, and compositions are important

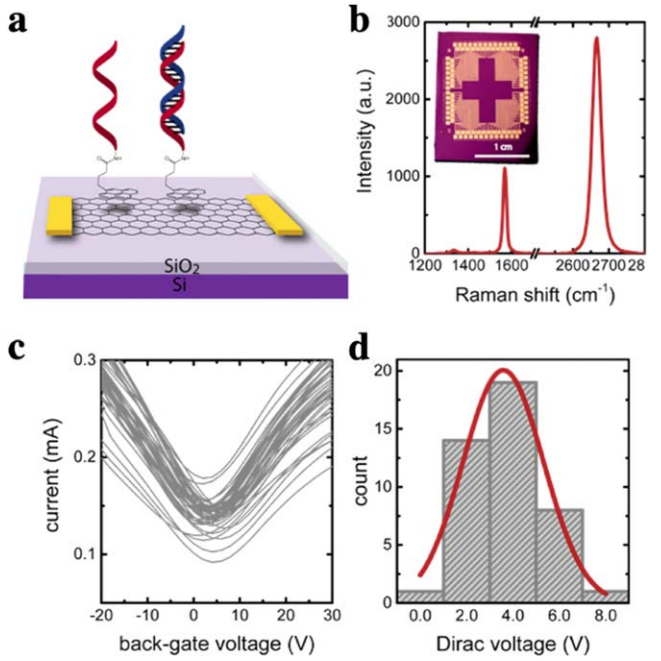

Figure 8. (a) Schematic of a DNA biosensor based on GFET device. (b) Raman measurements demonstrated single-layer graphene with a high-quality. (c) Typical transfer curve of 52 GFET array devices showing good reproducibility. (d) Histogram of the Dirac voltage obtained from transfer curve. Reprinted with permission from Ref. 183. Copyright 2016, American Chemical Society.

parameters to realize better performances.[189] Graphene has been utilized as NPs support and its large specific surface area (2630 m^2 g^{-1})[190] provides high loading of nanoparticles, high exposure of active sites, stability, and electron transfer rate.[191–193] A variety of nanoparticles can be modified to the surface of graphene either through covalent bond linkage or non-covalent functionalization (including van der Waals interactions, $\pi-\pi$ stacking, and electrostatic interactions.). The NPs attached to the graphene surface of GFET biosensor will increase available surface area for the binding of target biomolecules, intensify signals and rise the electrical conductivity.[194] For instance, the thiol groups are commonly used as a bio-recognition probes linker to Au NPs by taking advantage of the strong Au-S bonding.[195] Danielson and colleagues fabricated a lactose GFET biosensor based on CVD graphene decorated with Au NPs which further connected with the carbohydrate recognition domain.[196] It achieves a detection limit of 200 aM (Fig. 9b), which is much superior than electrochemical biosensors.

Due to the work function difference between graphene and contact metals, there will be electron diffusion resulted doping effect.[132] It tunes the electronic properties of graphene,[199] such as silver nanoparticles decorated graphene normal demonstrates typical n-type doping.[200] While Au/graphene exhibits strong morphology-dependence: with well dispersed Au nanoparticles indicates n-type doping and with continuous Au film indicates p-type doping (Fig. 9c).[197] Generally, the deposition of the nanoparticle yields a decrease in the mobility of graphene. However, accurate deposition sites control on graphene could realize the fine tune of charged impurities induced by metal nanoparticles.[201] Gao et al. reported that the GFET devices decorated with Au-NPs of 5.3 ± 1.2 nm demonstrated slightly reduced hole and electron mobility of 3590 ± 710 cm^2 V^{-1} s^{-1} and 1670 ± 230 cm^2 V^{-1} s^{-1}, respectively (Fig. 9d). After functionalized with thiolated-DNA, it realizes LOD of 1 nM with very high selectivity against non-complementary DNA.[198] Meanwhile, strong surface resonance Ag-NPs grafted graphene demonstrated much enhanced the electrical conductance by a factor of 2 to 4.[202] All of those discussed extraordinary properties of metal nanoparticle decorated graphene offer huge possibilities in developing GFET biosensors.

Applications of GFET Biosensors

GFET biosensors transduce biological signal directly to electronic signal that offers several advantages over traditional biosensors, including high spatial resolution, high sensitivities, miniature in size, label-free and non-destructive.[24,25,203] The GFET sensor configuration provides a versatile platform for a wide range of biosensing applications to the rapid growth of health care and scientific research, such as quick detection of pathogenic viruses,[204,205] cancer biomarkers,[206] physiological processes,[207] glucose,[79,208] protein,[209,210] and DNA.[211–214] In this section, we wish to focus our attention on the year of 2016–2021s, reviewing GFET-based biosensor studies.

We selected some representative reports and summarized the analyte target, functionalization method, sensing performance, electrolyte medium as well as graphene type in Table I. In recent years, GFET biosensors have been widely used in a variety of biological processes in the different sample medium. From the table, we concluded that GFET biosensors that utilize pristine monolayer CVD-grown graphene or exfoliated graphene, which possess high mobility, few defects, and preserve electrical properties as much as possible during the functionalization process demonstrated a better sensing response and detection limit. Compared with previous reports, recent GFET biosensors exhibit a better performance due to the utilization of advancements of graphene-based sensing technology. Their detection limit falls in the range of picomolar (pM) to femtomolar (fM) and even to the attomolar (aM) range.[158] These results support the aforementioned discussions on the structure of high-performance GFET biosensors. For example, in our listed cases of DNA detection, we made comparisons between sensing reactions based on DNA hybridizations with nearly equal lengths and comparable equilibrium dissociation constants. The DNA GFET biosensors with high mobility (2700 ± 700 cm^2 V^{-1} s^{-1}) demonstrated a lower detection limit in 5 fM for 21-mer DNA compared with 10 pM for 22-mer DNA even in a high ionic concentration. We also compare the same analyte target with different functionalization methods. The non-covalent modification preserves the electrical properties of graphene and thus exhibits a better detection limit, such as the case of insulin detections. Pyrene derivatives as linkers for the non-covalently connect to bio-recognition elements exhibit a better detection limit at 35 pM compared to 100 pM of the covalent functionalization.

In particular, the potential drop induced by the bio-recognition process on the gate electrode also demonstrated a low detection limit.[44,229] This kind of device structure is simple and easy to fabricate. Graphene merely acts as the channel material of the transistor and exhibits low power consumption. On the other hand, it can also achieve dual gate or multi-gate transistor detection structures that simultaneously sense multiple biomolecules. In addition, the channel sensing structure can also be recycled and reused.

We are noting that the comparison mentioned above may not be fair and accurate. The surface morphology, preparation quality, and test environment of each sensor are more or less different. These all affect the performance of the sensor. Therefore, for the comparison of the absolute sensor performance, we should conduct a detailed analysis case by case. The examples in the list just demonstrate the current development trend of GFET biosensors.

Glucose, protein, and DNA sensors.—Noncommunicable diseases, such as diabetes, cancer, and heart disease, are responsible for over 70% of all deaths worldwide.[248] Early detection of these disease biomarkers is highly desirable in clinical diagnostics. Application of GFET offers advantages of realizing point-of-care detection in a lower concentration of body fluid (saliva, tears, urine, etc.), in addition to be flexible and wearable.

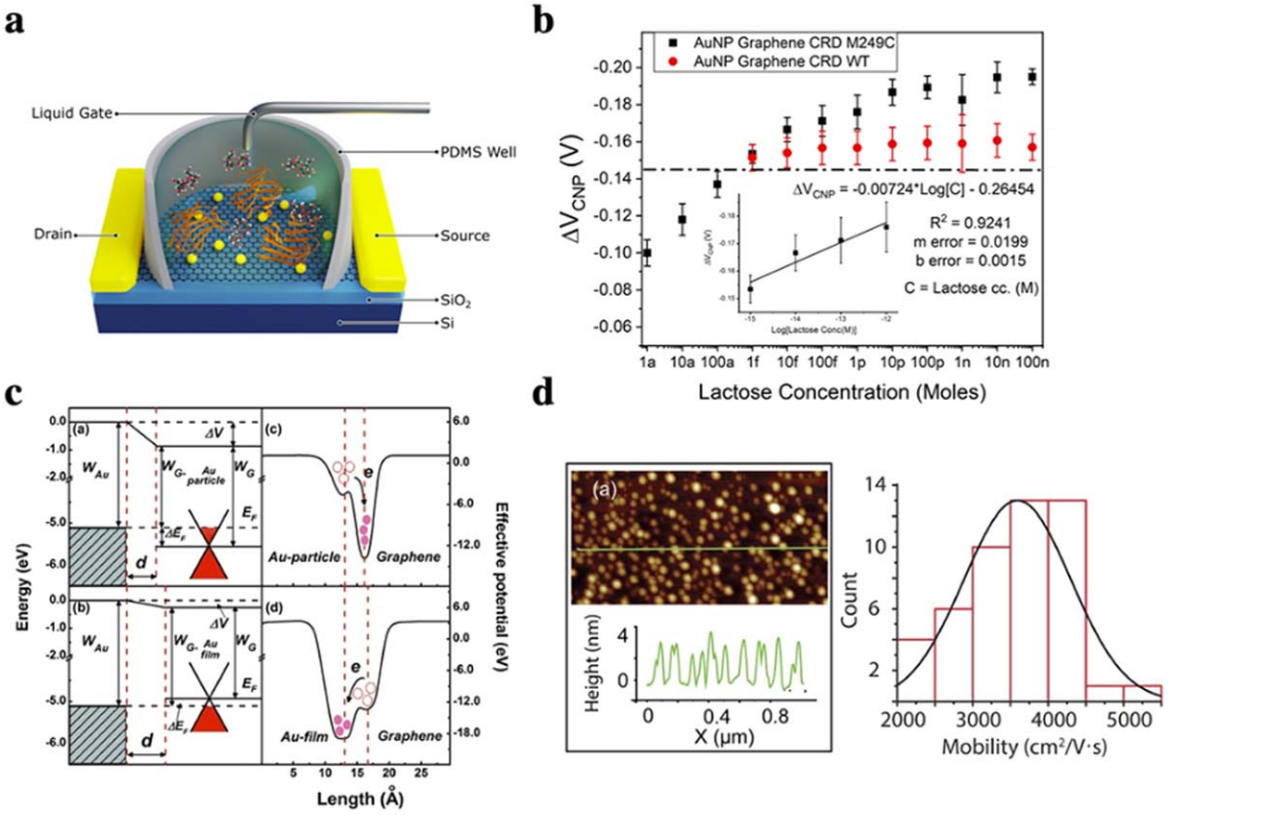

Figure 9. (a) Schematic diagram of a GFET biosensor for lactose detection. (b) The shift of Dirac point (V_{CNP}) as a function of lactose concentration from 1 aM to 100 pM. The black squares represent GFET functionalized with hGal-3 M249C mutant and the red circles represent CRD wildtype. Inset: the dynamic range of lactose GFET sensor between 1 fM and 1 pM. Reprinted with permission from Ref. 196. Copyright 2019, Elsevier. (c) A band alignment schematic illustration of graphene-Au nanoparticle and graphene-Au film. Reprinted with permission from Ref. 197. Copyright 2012, John Wiley and Sons. (d) A typical AFM image of Au nanoparticles decorated graphene. The corresponding AFM line shown below demonstrated a good uniformity. On the right side, histograms of hole mobility with Gaussian fits of 24 Au nanoparticles decorated GFET devices on three separate arrays. Reprinted with permission from Ref. 198. Copyright 2014, American Chemical Society.

Glucose sensing.—Non-enzymatic sensors could play a new role in the sensing of glucose, which can effectively solve the problem that the lack of long-time stability of enzymes.[249] Dong et al. realized the non-enzymatic sensing of glucose by electrodeposition of palladium nanoflower on the channel surface of the GFET-type sensor. Further, nafion layer and glucose oxidase was used to improve the selectivity of the sensor. The detection limit of the GFET glucose biosensor was 1 nM with excellent selectivity against uric and ascorbic acid. The result indicates that the morphology of platinum flowers has a great influence on the sensitivity of glucose.

Xiong et al. presented a novel GFET biosensor that could detect glucose and UA (uric acid) simultaneously.[229] CVD graphene was utilized as channel material and two separate Au gate electrodes were modified with GOx-chitosan and BSA-chitosan respectively. Its sensitivity was dramatically improved to 100 nM after latterly co-modified by porous Co_3O_4 hollow nanopolyhedrons, which is beyond the detection range required by tears and was successfully used to analyze a real tear sample. The sensing mechanism for the glucose is attributed to the electrocatalysis of the H_2O_2 generated by oxidation of glucose near the gate electrode, as for uric acid the response is mainly caused by direct oxidation on the surface of gate electrode.

Cancer biomarker detection.—Lin and colleagues fabricated a GFET biosensor modified with the antibody for label-free cancer biomarker (CEA) detection.[233] The antibodies targeting carcinoembryonic antigen (Anti-CEA) were non-covalently decorated on the graphene surface via PYR-NHS linker. The fabricated sensor demonstrated specificity against interferons and a LOD of less than 100 pg ml^{-1}. They also estimated the dissociation constant between CEA protein and anti-CEA is 6.35×10^{-11} M, showing a high selectivity to target cancer biomarker protein.

In recent years, more evidence has demonstrated that exosomes are related to pathological processes such as tumorigenesis, metastasis, and cancer progression.[250] It can be used as biomarkers for early cancer diagnosis. Ramadan et al. constructed a CVD graphene-based FET biosensor for exosomes detection.[234] The CD63 antibody bioreceptor was functionalized with a PBASE linker. Compared with the bare graphene channel, the graphene decorating with carbon dots exhibits three orders of magnitude enhancement in sensing performance. The LOD of exosome detection was down to 100 particles μl^{-1}. The heterogeneous structure formed by carbon dots decorated graphene without distorting the aromaticity of the graphene lattice has significantly improved the detection limit of the GFET biosensor.

Gene detection.—Recently, Clustered Regularly Interspaced Short Palindromic Repeats (CRISPR)-associated nuclease (Cas) related technology has been integrated with graphene for the detection of unamplified target genes. Hajian et al. developed a CRISPR-Chip for digital and label-free nucleic acid testing of the target sequence within intact genomic material.[121] Catalytically deactivated CRISPR-associated protein 9 (Cas9) complex, denoted as dRNP and possesses the gene-targeting capacity, combined with a specific single-guide RNA was non-covalent immobilized on the graphene surface. The dRNP scans the entire genomic sample until it binds to the target sequence that is complementary to the single-guide RNA molecule (sgRNA) within dRNP. The hybridization process of the target DNA affects mobility, thereby enabling accurate electrical signal detection. The fabricated CRISPR-Chip

Table I. Comparison of the sensing performances of the GFETs for different analytes

Analyte type	Target	Functionalization method	Detection limit	Electrolyte medium	Graphene type, References
Genes	DNA methylation	PBASE		2 mM $MgCl_2$/30 mM Tris	CVD[215]
	TP53 DNA cancer-related gene		1 nM	10 mM PBS	CVD[125]
	HIV virus related 11-mer ssDNA	Lys (Pyrene)	4 pM	1 mM PBS	CVD[216]
	15-mer DNA	PBASE	1 aM	PBS	CVD (photocurrent modulated)[217]
	20-mer DNA	Poly (L-lysine)	10 fM	1 mM PBS	CVD[218]
	21-mer DNA	PBASE	5 fM	50 mM SSC[a)]	LP-CVD[219]
	22-mer DNA	PBASE	10 pM	0.1 mM PBS	CVD[220]
	25-nt DNA	PBASE with NHS reaction	25 aM	10 mM PB	CVD[221]
	60-mer DNA	PBASE	1 fM	DI water	CVD[183]
	Target DNA	Thiol bond on AuNPs	1 nM	DI water	LP-CVD[198]
	Target DNA	Thiol bond on **gate electrode**	1 fM	PBS	CVD[44]
	Target DNA	PBASE	100 fM	10 mM PBS	CVD[222]
	Target DNA	Plasma treated PBASE	10 aM	PBS	CVD[223]
	Specific single-guide RNA	PBA[b)]	1.7 fM	2 mM $MgCl_2$	CVD[121]
	miRNA	Absorbed	10 fM	10 mM PBS	CVD[224]
Protein	Insulin	PBASE	35 pM	PBS	CVD[124]
	Insulin	Diazonium chemistry	100 pM	PBS	CVD[225]
	IgE	PBASE	47 pM	0.1 mM PBS	CVD[226]
	TNF-α	PBASE	5 pM	10 mM PBS	CVD[187]
	Hemin	Absorbed	10 nM	PBS	CVD[227]
Carbohydrate	Glucose	Palladium nanoflower GOx/Nafion	1 nM	1 M NaOH/0.1 M PBS	CVD[228]
	Glucose	GOx-chitosan and Co_3O_4 nanopolyhedron on **gate electrode**	100 nM	100 mM PBS	CVD[229]
	Lactose	Thiol bond	200 aM	0.1 mM PBS	CVD[196]
Virus	SARS-CoV-2	PBASE	PBS: 16 pfu ml^{-1}	PBS and clinical samples	CVD[230]
			Clinical sample: 242 copies ml^{-1}		
	Influenza and SARS-CoV-2	MXene with APTES	125 copies ml^{-1} and 1 fg ml^{-1}	10 mM PBS	CVD[231]
	HIV CVDs and RA	EDS/NHS	p24:100 fg ml^{-1} cTn1:10 fg ml^{-1}	50 mM PB	Exfoliated[166]
	Zika virus	NHS	40 pM	10 mM PBS	CVD[232]
Cancer biomarker	H. pylori cells	PBASE	270 zM	100 mM PB	Exfoliated[155]
	CEA	PYR-NHS	100 pg ml^{-1}	1 μM PBS	CVD[233]
	8-OHDG	Diazotization	0.35 nM	PBS	Epitaxial[167]
	Exosome	PBASE	100 particles μl^{-1}	0.01 mM PBS	CVD[234]
Bacteria	Antibiotic resistant bacteria	Pyrene-based linker	10^4 cells ml^{-1}	0.1 mM PBS	CVD[235]

Table I. (Continued).

Analyte type	Target	Functionalization method	Detection limit	Electrolyte medium	Graphene type, References
	Borrelia burgdorferi	PBASE	2 pg ml^{-1}	0.75 mM dialysis buffer	CVD[236]
Biomolecular	Neuropeptide Y	PBASE	10 pM	Tris	CVD[237]
	Biotin	PBASE	0.37 pM	PBS	CVD[238]
	ATP	PBASE	0.5 pM	DI water	CVD[239]
	7 amino acids	PBASE	10 fg ml^{-1}	10 mM PB	CVD[240]
	Bisphenol A	Thiol bond	10 ng ml^{-1}	PBS	CVD[241]
	Imatinib	PBASE	15.5 fM	2.5 mM Tris/1 mM $MgCl_2$	CVD[242]
	Histamine	AuNPs on gate electrode	100 nM	100 mM PBS	CVD[243]
	Methyl parathion	ZrO_2/rGO on gate electrode	10 pg ml^{-1}	0.2 M ABS	CVD[244]
Enantioselective	Chiral of β-citronellol	Boc-L-Phe-Pyrene	1.45 ppm for *R* 1.06 ppm for *S*	Analyte vapor	CVD[245]
Physiological process	Hemostasis process			PBS	CVD[246]
	Umami and sweet	PSE[c)]	100 nM for umami 1 uM for sweet	Dulbecco's PBS	CVD[247]

a) SCC: Saline-sodium citrate buffer. b) PBA: 1-pyrenebutanoic acid. c) PSE: *N*-hydroxysuccinimide ester.

was utilized in the detection of target DNA samples from HEK293T cell lines and clinical samples of DNA with two distinct mutations. In the target gene contained DNA solution, a sensitivity of 1.7 fM was achieved within 15 min without the need for a complicated amplification process. The combination of the GFET biosensor and CRISPR technology opens a new path for its future clinical genetic inspection.

Emerging biomolecular detection and life science applications.—Since Marburg virus and Ebola virus were firstly recognized in 1967,[251] more than 40 contagious viruses have been discovered, including HIV,[252] SARS,[253] MERS,[254] chikungunya,[255] avian flu,[256] swine flu,[257] Zika,[258] and the most recent one is so-called coronavirus or COVID-19.[259] Reliable and high-speed diagnostic tools are essential for stopping the spreading of virus and vaccine development. In life science, the application of GFETs provides new tools for analyzing pathological causes and monitoring human physiological processes. Afahi et al. presented a GFET biosensor for Zika virus detection.[232] They covalently functionalized graphene channel with monoclonal antibodies (Anti-Zika NS1). The antibody response to the electronegative Zika viral antigen molecule resulted in a change in the capacitance, achieving a detection limit of 450 pM in the buffer solution. Seo et al. have developed a GFET biosensor for rapid and accurate detection of SARS-CoV-2 in clinical samples.[230] The specific antigen against the SARS-CoV2 spike protein (anti-SARS-CoV-2) was immobilized on the graphene surface via PBASE as a non-covalent probe linker. Performance of this sensor was measured with antigen protein, cultured virus, and nasal swab specimens from COVID-19 patients. The GFET biosensor could detect the SARS-CoV-2 spike protein at concentrations of 1.31×10^{-5} pM in buffer solution and 1.31×10^{-3} pM in the biological fluid of the clinical samples. The sensor was further tested with viral strains in clinical samples and achieved a low limit detection in 2.42 g ml^{-1}. It is worth mentioning that the fabricated GFET biosensor exhibited no measurable cross-reactivity with the MERS-CoV antigen, demonstrating a good selectivity.

Wang et al. fabricated a flexible and stretchable field-effect transistor biosensor for TNF-α (inflammatory cytokine biomarker) detection.[187] The device is based on a 2.5 um thick mylar substrate that possesses a high level of mechanical flexibility and durability. The detection mechanism lies in measuring the change in the carrier concentration of the graphene induced by the specific binding of the aptamer with the target biomarker. The functionalized graphene with a carrier mobility of up to 3544 ± 231 $cm^2\ V^{-1}\ s^{-1}$. A series of bending, twisting, and stretching tests were performed to show that the sensor incurred no visible mechanical damage while retaining highly consistent electrical properties and biomarker responses. The fabricated flexible biosensor is capable of detection of TNF-α protein, with a low detection limit of 5 pM. The results demonstrated that GFET biosensors based on a flexible mylar substrate have the potential for consistent and reliable detection of liquid-borne biomarkers on human skin or tissue surfaces, as well as further expansion to wearable and implantable applications.

In recent years, GFET biosensors have also achieved breakthroughs in the detection of human physiological signals. Graphene is suitable for flexible sensor devices to achieve real-time wearable detection which hard for traditional silicon-based sensors on a rigid substrate. GFET biosensors are implanted into organisms for life signals detection. Masvidal-Codina et al. exploited GFET arrays for both the epicortical and intracortical mapping of cortical spreading depression (CSD).[260] CSD, a slowly propagating wave of near-complete depolarization of neurons and astrocytes followed by a period of electrical activity suppression, occurs at infraslow frequencies, which are usually aroused in the patients suffering from stroke, brain injury, and migraines. Recent research has also found that CSD plays a significant role in brain pathophysiology. The implantable GFET arrays are used to map CSD in rats and demonstrated that the sensor could record infraslow signals with high fidelity and signals in the typical local field potential bandwidth. The monitoring of infraslow brain activity by GFET arrays has the potential to further our understanding of brain function in health and disease to provide the most effective care possible.

GFET biosensors are also used in other life science research, such as monitoring the hemostasis process of human blood,[246] discriminating enantiomers,[245,261] duplex bioelectronic "tongues" that can distinguish umami and sweet flavors,[247] and so on. In addition, GFETs demonstrate an outstanding sensitivity in high-frequency response. GFETs exhibit a signal-to-noise ratio similar to platinum black electrodes in the frequency range below 100 Hz, up to the highest limit recorded of 1 kHz.[37] Compared with the PEDOT:PSS OECTs, which is considered a state-of-the-art flexible high-frequency detection material, graphene exhibits similar performance and has advantages in terms of gate response frequency and power consumption. These advantages allow GFET biosensors have a good performance in neural sensing. For recent reviews beyond the scope of this work, the reader can refer to the following: The Harmonic Distortion and Non-Ideal Frequency Response in g-SGFETs,[262] Frequency-Division Multiplexing of Neural Signals by Graphene Sensors,[90] and Mapping of Brain Electrical Activity with the Flexible SGFETs Array.[263] These results indicate that GFET biosensors will become a very powerful sensing platform, whether for the detection of biomolecules or for life vital signals.

Perspectives and Conclusions

In this article, we have reviewed the strategies in constructing graphene-based FET biosensors and summarized the current applications. We highlighted recent research advances in the preparation of high-quality graphene, the interaction between graphene and substrates, graphene defects and their consequences related to electrochemistry, metal electrode contacts, and Debye screening length engineering, as well as functionalization of GFET. Although well-designed GFET biosensors have been applied in various forms for human-based biomolecule detection, which have realized at the proof of concept level demonstrating a bright research prospect. There is still room for improving GFET biosensor industrialization and commercial application.

Firstly, high-quality graphene is ideal for GFET fabrications. The higher mobility has demonstrated a larger sensing response and reduced electrical noise both theoretically and experimentally. Recently, graphene-based electronic devices with an average mobility of 5 000 $cm^2\ V^{-1}\ s^{-1}$ have been reported. However, the electronic transport performance in GFET biosensors has not yet reached this level. Therefore, some new techniques can be applied to the manufacture of GFET biosensors to achieve higher mobility. For instance, improving electrical properties by using h-BN as a dielectric substrate. The establishment of graphene industrial quality control standards and the development of graphene industrial synthesis are necessary for the commercialization and manufacturability of GFET biosensors.[264,265]

Secondly, Although there are some commercial biotechnology companies provide GFET-based detection platforms for biosensing research.[266] For instance, Graphenea is a company focused on high-quality graphene device fabrication for customers sensing applications. Another company called Nanomedical Diagnostics also provides a graphene based FET biosensing platform (Agile R100 binding assay system) for real-time detection of small biomolecules. Thus, additional efforts are needed to develop a more stable graphene interface functionalization method, which obtains reliable biorecognition signals not only in controlled laboratory conditions but also the complex practical environment. The design of bioreceptor surface chemistry can overcome Debye length and improve the repeatability for multiple biological target molecules in multiomics studies.[31] Further, sufficient replicas combine with machine learning and intelligent analytics become more and more critical.[65,267]

Thirdly, in terms of truly achieving a scalable production, GFET biosensors based on 2D morphology could be integrated with the

microelectronics fabrication process to develop high-density sensor arrays. A multi-transistor device system connected with designed firmware is required for multiplexing sensing instead of repeated individual measurements, which improves stability and reproducibility.[65] Moreover, there is the possibility of developing high-density arrays for simultaneous analyses of multiple species in small sample volumes. The design scheme of multi-device arrays is simplifying the analysis procedure and improving the detection efficiency. At the same time, the analysis and processing of the measured raw signal can be addressed in the common electronic products such as mobile phones through wireless transmission,[268,269] which can improve the ease of use and practical applicability of the GFET sensors.

In summary, graphene is expected to serve as the channel material for next-generation high-performance FET biosensors. GFET biosensors have been explored in a variety of biosensing applications, as well as further extend their application into life science studies. Although GFET biosensors show promise, commercial products are yet to come. There is still a need for breakthroughs in sensor development, either for enhancing GFET stability, reproducibility, improving selectivity in real testing processes or developing more creative graphene sensor fabrication methods. We firmly believe that with continued efforts GFET biosensors will have a significant and bright future.

Acknowledgments

This work was financially supported by the National Natural Science Foundation of China (No. 11774255) and the National Basic Research Program of China (2020YFC2004602).

Declaration of Competing Interest

The authors declare that they have no known competing financial interests or personal relationships that could have appeared to influence the work reported in this paper.

ORCID

Yanqing Ma https://orcid.org/0000-0002-3317-8273

References

1. N. Wongkaew, M. Simsek, C. Griesche, and A. J. Baeumner, *Chem. Rev.*, **119**, 120 (2019).
2. H. Craighead, *Nature*, **442**, 387 (2006).
3. F. Schedin, A. K. Geim, S. V. Morozov, E. W. Hill, P. Blake, M. I. Katsnelson, and K. S. Novoselov, *Nat. Mater.*, **6**, 652 (2007).
4. W. Fu, L. Jiang, E. P. van Geest, L. M. C. Lima, and G. F. Schneider, *Adv. Mater.*, **29**, 1603610 (2017).
5. A. Heilig, N. Bârsan, U. Weimar, M. Schweizer-Berberich, J. W. Gardner, and W. Göpel, *Sens. Actuators, B*, **43**, 45 (1997).
6. M. Chhowalla, D. Jena, and H. Zhang, *Nat. Rev. Mater.*, **1**, 16052 (2016).
7. J. Kang, W. Cao, X. Xie, D. Sarkar, W. Liu, and K. Banerjee, *Graphene and Beyond-Graphene 2D Crystals for Next-Generation Green Electronics* (SPIE, USA) 9083, 1 (2014).
8. D. Jena, *Proc. IEEE*, **101**, 1585 (2013).
9. Z. J. Han, H. Mehdipour, X. Li, J. Shen, L. Randeniya, H. Y. Yang, and K. Ostrikov, *ACS Nano*, **6**, 5809 (2012).
10. Y. Cui, Q. Wei, H. Park, and C. M. Lieber, *Science*, **293**, 1289 (2001).
11. N. S. Ramgir, Y. Yang, and M. Zacharias, *Small*, **6**, 1705 (2010).
12. S. Mao, J. Chang, H. Pu, G. Lu, Q. He, H. Zhang, and J. Chen, *Chem. Soc. Rev.*, **46**, 6872 (2017).
13. A. K. Geim and K. S. Novoselov, *Nat. Mater.*, **6**, 183 (2007).
14. S. Das Sarma, S. Adam, E. H. Hwang, and E. Rossi, *Rev. Mod. Phys.*, **83**, 407 (2011).
15. D. H. Tien, J.-Y. Park, K. B. Kim, N. Lee, T. Choi, P. Kim, T. Taniguchi, K. Watanabe, and Y. Seo, *ACS Appl. Mater. Interfaces*, **8**, 3072 (2016).
16. L. Wang et al., *Science*, **342**, 614 (2013).
17. X. Du, I. Skachko, A. Barker, and E. Y. Andrei, *Nat. Nanotechnol.*, **3**, 491 (2008).
18. F. Schwierz, *Nat. Nanotechnol.*, **5**, 487 (2010).
19. S. M. Sze, Y. Li, and K. K. Ng, *Physics of Semiconductor Devices* (Wiley, New York, NY) 3rd ed., p. 832 (2007).
20. M. S. Fuhrer and J. Hone, *Nat. Nanotechnol.*, **8**, 146 (2013).
21. W. Fu, C. Nef, O. Knopfmacher, A. Tarasov, M. Weiss, M. Calame, and C. Schonenberger, *Nano Lett.*, **11**, 3597 (2011).
22. A. Stergiou, R. Canton-Vitoria, M. N. Psarrou, S. P. Economopoulos, and N. Tagmatarchis, *Prog. Mater Sci.*, **114**, 100683 (2020).
23. P. T. Yin, S. Shah, M. Chhowalla, and K. B. Lee, *Chem. Rev.*, **115**, 2483 (2015).
24. Z. Jiang, B. Feng, J. Xu, T. Qing, P. Zhang, and Z. Qing, *Biosens. Bioelectron.*, **166**, 112471 (2020).
25. E. Vermisoglou, D. Panáček, K. Jayaramulu, M. Pykal, I. Frébort, M. Kolář, M. Hajdúch, R. Zbořil, and M. Otyepka, *Biosens. Bioelectron.*, **166**, 112436 (2020).
26. E. Singh, M. Meyyappan, and H. S. Nalwa, *ACS Appl. Mater. Interfaces*, **9**, 34544 (2017).
27. X. Zhang, Q. Jing, S. Ao, G. F. Schneider, D. Kireev, Z. Zhang, and W. Fu, *Small*, **16**, 1902820 (2020).
28. B. Zhan, C. Li, J. Yang, G. Jenkins, W. Huang, and X. Dong, *Small*, **10**, 4042 (2014).
29. A. Ambrosi, C. K. Chua, N. M. Latiff, A. H. Loo, C. H. A. Wong, A. Y. S. Eng, A. Bonanni, and M. Pumera, *Chem. Soc. Rev.*, **45**, 2458 (2016).
30. I.-Y. Sohn, D.-J. Kim, J.-H. Jung, O. J. Yoon, T. Nguyen Thanh, T. Tran Quang, and N.-E. Lee, *Biosens. Bioelectron.*, **45**, 70 (2013).
31. A. Béraud, M. Sauvage, C. M. Bazán, M. Tie, A. Bencherif, and D. Bouilly, *Analyst*, **146**, 403 (2021).
32. J. T. Robinson, F. K. Perkins, E. S. Snow, Z. Wei, and P. E. Sheehan, *Nano Lett.*, **8**, 3137 (2008).
33. S. Pei and H.-M. Cheng, *Carbon*, **50**, 3210 (2012).
34. Z. Meng, R. M. Stolz, L. Mendecki, and K. A. Mirica, *Chem. Rev.*, **119**, 478 (2019).
35. Q. Fan, L. Wang, D. Xu, Y. Duo, J. Gao, L. Zhang, X. Wang, X. Chen, J. Li, and H. Zhang, *Nanoscale*, **12**, 11364 (2020).
36. N. Lu, L. Wang, M. Lv, Z. Tang, and C. Fan, *Nano Res.*, **12**, 247 (2019).
37. C. Hébert et al., *Adv. Funct. Mater.*, **28**, 1703976 (2018).
38. E. Uesugi, H. Goto, R. Eguchi, A. Fujiwara, and Y. Kubozono, *Sci. Rep.*, **3**, 1595 (2013).
39. F. Chen, Q. Qing, J. Xia, J. Li, and N. Tao, *J. Am. Chem. Soc.*, **131**, 9908 (2009).
40. J. Xia, F. Chen, J. Li, and N. Tao, *Nat. Nanotechnol.*, **4**, 505 (2009).
41. S. Z. Bisri, S. Shimizu, M. Nakano, and Y. Iwasa, *Adv. Mater.*, **29**, 1607054 (2017).
42. J. B. Allen and R. F. Larry, *Electrochemical Methods Fundamentals and Applications* (Wiley, New York, NY) (2001).
43. E. D. Minot, A. M. Janssens, I. Heller, H. A. Heering, C. Dekker, and S. G. Lemay, *Appl. Phys. Lett.*, **91**, 093507 (2007).
44. S. Li, K. Huang, Q. Fan, S. Yang, T. Shen, T. Mei, J. Wang, X. Wang, G. Chang, and J. Li, *Biosens. Bioelectron.*, **136**, 91 (2019).
45. J. Rivnay, S. Inal, A. Salleo, R. M. Owens, M. Berggren, and G. G. Malliaras, *Nat. Rev. Mater.*, **3**, 17086 (2018).
46. G. Xu, J. Abbott, L. Qin, K. Y. Yeung, Y. Song, H. Yoon, J. Kong, and D. Ham, *Nat. Commun.*, **5**, 4866 (2014).
47. P. Fromherz, A. Offenhausser, T. Vetter, and J. Weis, *Science*, **252**, 1290 (1991).
48. B. M. Blaschke, M. Lottner, S. Drieschner, A. B. Calia, K. Stoiber, L. Rousseau, G. Lissourges, and J. A. Garrido, *2D Mater.*, **3**, 025007 (2016).
49. D. R. Cooper, B. D'Anjou, N. Ghattamaneni, B. Harack, M. Hilke, A. Horth, N. Majlis, M. Massicotte, L. Vandsburger, and E. Whiteway, *ISRN Condens. Matter Phys.*, **2012**, 501686 (2012).
50. K. S. Novoselov, V. I. Fal'ko, L. Colombo, P. R. Gellert, M. G. Schwab, and K. Kim, *Nature*, **490**, 192 (2012).
51. K. S. Novoselov, A. K. Geim, S. V. Morozov, D. Jiang, Y. Zhang, S. V. Dubonos, I. V. Grigorieva, and A. A. Firsov, *Science*, **306**, 666 (2004).
52. G. Auton, J. Zhang, R. K. Kumar, H. Wang, X. Zhang, Q. Wang, E. Hill, and A. Song, *Nat. Commun.*, **7**, 11670 (2016).
53. C. Berger et al., *J. Phys. Chem. B*, **108**, 19912 (2004).
54. M. Orlita, C. Faugeras, R. Grill, A. Wysmolek, W. Strupinski, C. Berger, W. A. de Heer, G. Martinez, and M. Potemski, *Phys. Rev. Lett.*, **107**, 216603 (2011).
55. C. Berger, E. Conrad, and de H. Walt, "Epigraphene: epitaxial graphene on silicon carbide." *Physics of Solid Surfaces, Subvolume B,* (Spinger, Berlin) (2018).
56. D. S. Lee, C. Riedl, B. Krauss, K. von Klitzing, U. Starke, and J. H. Smet, *Nano Lett.*, **8**, 4320 (2008).
57. J. Kim, H. Park, J. B. Hannon, S. W. Bedell, K. Fogel, D. K. Sadana, and C. Dimitrakopoulos, *Science*, **342**, 833 (2013).
58. J. A. Robinson, M. Hollander, M. Labella, K. A. Trumbull, R. Cavalero, and D. W. Snyder, *Nano Lett.*, **11**, 3875 (2011).
59. L. Lin, B. Deng, J. Y. Sun, H. L. Peng, and Z. F. Liu, *Chem. Rev.*, **118**, 9281 (2018).
60. J. Zhang, L. Lin, K. Jia, L. Sun, H. Peng, and Z. Liu, *Adv. Mater.*, **32**, 1903266 (2020).
61. Q. H. Wang et al., *Nat. Chem.*, **4**, 724 (2012).
62. L. Banszerus, M. Schmitz, S. Engels, J. Dauber, M. Oellers, F. Haupt, K. Watanabe, T. Taniguchi, B. Beschoten, and C. Stampfer, *Sci. Adv.*, **1**, 1500222 (2015).
63. C. R. Dean et al., *Nat. Nanotechnol.*, **5**, 722 (2010).
64. B. N. Chandrashekar, B. Deng, A. S. Smitha, Y. Chen, C. Tan, H. Zhang, H. Peng, and Z. Liu, *Adv. Mater.*, **27**, 5210 (2015).
65. H.-W. Lu, A. A. Kane, J. Parkinson, Y. Gao, R. Hajian, M. Heltzen, B. Goldsmith, and K. Aran, *Biosens. Bioelectron.*, **195**, 113605 (2021).
66. X. Y. Fan, R. Nouchi, and K. Tanigaki, *J. Phys. Chem. C*, **115**, 12960 (2011).
67. K. M. Burson, W. G. Cullen, S. Adam, C. R. Dean, K. Watanabe, T. Taniguchi, P. Kim, and M. S. Fuhrer, *Nano Lett.*, **13**, 3576 (2013).
68. F. Gao, H. Yang, and P. Hu, *Small Methods*, **2**, 1700384 (2018).
69. K. I. Bolotin, K. J. Sikes, Z. Jiang, M. Klima, G. Fudenberg, J. Hone, P. Kim, and H. L. Stormer, *Solid State Commun.*, **146**, 351 (2008).
70. W. H. Lee and Y. D. Park, *Adv. Mater. Interfaces*, **5**, 1700316 (2018).

71. M. Lafkioti, B. Krauss, T. Lohmann, U. Zschieschang, H. Klauk, K. V. Klitzing, and J. H. Smet, *Nano Lett.*, **10**, 1149 (2010).
72. X. Wang, J.-B. Xu, C. Wang, J. Du, and W. Xie, *Adv. Mater.*, **23**, 2464 (2011).
73. C. H. Yeh et al., *Biosens. Bioelectron.*, **77**, 1008 (2016).
74. D. De Fazio et al., *ACS Nano*, **13**, 8926 (2019).
75. Y. Liu, S. Bhowmick, and B. I. Yakobson, *Nano Lett.*, **11**, 3113 (2011).
76. K. Watanabe, T. Taniguchi, and H. Kanda, *Nat. Mater.*, **3**, 404 (2004).
77. T. A. Chen et al., *Nature*, **579**, 219 (2020).
78. J. Lee, T. J. Ha, H. Li, K. N. Parrish, M. Holt, A. Dodabalapur, R. S. Ruoff, and D. Akinwande, *ACS Nano*, **7**, 7744 (2013).
79. Y. H. Kwak, D. S. Choi, Y. N. Kim, H. Kim, D. H. Yoon, S.-S. Ahn, J.-W. Yang, W. S. Yang, and S. Seo, *Biosens. Bioelectron.*, **37**, 82 (2012).
80. H. Yoon, J. Nah, H. Kim, S. Ko, M. Sharifuzzaman, S. C. Barman, X. Xuan, J. Kim, and J. Y. Park, *Sens. Actuators, B*, **311**, 127866 (2020).
81. L. G. Martins, Y. Song, T. Zeng, M. S. Dresselhaus, J. Kong, and P. T. Araujo, *Proc. Natl. Acad. Sci. U. S. A.*, **110**, 17762 (2013).
82. F. Z. Qing, Y. F. Zhang, Y. T. Niu, R. Stehle, Y. F. Chen, and X. S. Li, *Nanoscale*, **12**, 10890 (2020).
83. G. Borin Barin, Y. Song, I. de Fátima Gimenez, A. G. Souza Filho, L. S. Barreto, and J. Kong, *Carbon*, **84**, 82 (2015).
84. V. Geringer, D. Subramaniam, A. K. Michel, B. Szafranek, D. Schall, A. Georgi, T. Mashoff, D. Neumaier, M. Liebmann, and M. Morgenstern, *Appl. Phys. Lett.*, **96**, 082114 (2010).
85. Y. Y. Wang and P. J. Burke, *Appl. Phys. Lett.*, **103**, 052103 (2013).
86. Y. P. Hsieh, C. L. Kuo, and M. Hofmann, *Nanoscale*, **8**, 1327 (2016).
87. Y. Liang, X. Liang, Z. Zhang, W. Li, X. Huo, and L. Peng, *Nanoscale*, **7**, 10954 (2015).
88. W. S. Leong et al., *Nat. Commun.*, **10**, 867 (2019).
89. S. Sheibani, L. Capua, S. Kamaei, S. S. A. Akbari, J. Zhang, H. Guerin, and A. M. Ionescu, *Commun. Mater.*, **2**, 10 (2021).
90. R. Garcia-Cortadella et al., *Nano Lett.*, **20**, 3528 (2020).
91. M. H. Gass, U. Bangert, A. L. Bleloch, P. Wang, R. R. Nair, and A. K. Geim, *Nat. Nanotechnol.*, **3**, 676 (2008).
92. A. Eckmann, A. Felten, A. Mishchenko, L. Britnell, R. Krupke, K. S. Novoselov, and C. Casiraghi, *Nano Lett.*, **12**, 3925 (2012).
93. M. Tripathi, F. Awaja, R. A. Bizao, S. Signetti, E. Iacob, G. Paolicelli, S. Valeri, A. Dalton, and N. M. Pugno, *ACS Appl. Mater. Interfaces*, **10**, 44614 (2018).
94. A. Zandiatashbar, G. H. Lee, S. J. An, S. Lee, N. Mathew, M. Terrones, T. Hayashi, C. R. Picu, J. Hone, and N. Koratkar, *Nat. Commun.*, **5**, 3186 (2014).
95. A. Das, B. Chakraborty, and A. K. Sood, *Bull. Mater. Sci.*, **31**, 579 (2008).
96. F. Banhart, J. Kotakoski, and A. V. Krasheninnikov, *ACS Nano*, **5**, 26 (2011).
97. B. Kumar et al., *Nano Lett.*, **13**, 1962 (2013).
98. R. Beams, L. Gustavo Cançado, and L. Novotny, *J. Phys. Condens. Matter*, **27**, 083002 (2015).
99. C. Shan, H. Yang, J. Song, D. Han, A. Ivaska, and L. Niu, *Anal. Chem.*, **81**, 2378 (2009).
100. C. X. Lim, H. Y. Hoh, P. K. Ang, and K. P. Loh, *Anal. Chem.*, **82**, 7387 (2010).
101. G. Froehlicher and S. Berciaud, *Phys. Rev. B*, **91**, 205413 (2015).
102. C. Tan, J. Rodriguez-Lopez, J. J. Parks, N. L. Ritzert, D. C. Ralph, and H. D. Abruna, *ACS Nano*, **6**, 3070 (2012).
103. J. H. Zhong, J. Zhang, X. Jin, J. Y. Liu, Q. Y. Li, M. H. Li, W. W. Cai, D. Y. Wu, D. P. Zhan, and B. Ren, *J. Am. Chem. Soc.*, **136**, 16609 (2014).
104. Y. Zhou, M. Ma, H. He, Z. Cai, N. Gao, C. He, G. Chang, X. Wang, and Y. He, *Biosens. Bioelectron.*, **146**, 111751 (2019).
105. W. Fu, L. Feng, G. Panaitov, D. Kireev, D. Mayer, A. Offenhausser, and H. J. Krause, *Sci. Adv.*, **3**, 1701247 (2017).
106. X. Zhang, Y. Zhang, Q. Liao, Y. Song, and S. Ma, *Small*, **9**, 4045 (2013).
107. S. Borini, R. White, D. Wei, M. Astley, S. Haque, E. Spigone, N. Harris, J. Kivioja, and T. Ryhänen, *ACS Nano*, **7**, 11166 (2013).
108. T. Wu, A. Alharbi, R. Kiani, and D. Shahrjerdi, *Adv. Mater.*, **31**, 1805752 (2019).
109. Y. Wang, Y. Zheng, X. Xu, E. Dubuisson, Q. Bao, J. Lu, and K. P. Loh, *ACS Nano*, **5**, 9927 (2011).
110. P. Szroeder, N. G. Tsierkezos, M. Walczyk, W. Strupinski, A. Gorska-Pukownik, J. Strzelecki, K. Wiwatowski, P. Scharff, and U. Ritter, *J. Solid State Electrochem.*, **18**, 2555 (2014).
111. W. Li, C. Tan, M. A. Lowe, H. D. Abruna, and D. C. Ralph, *ACS Nano*, **5**, 2264 (2011).
112. A. T. Valota, I. A. Kinloch, K. S. Novoselov, C. Casiraghi, A. Eckmann, E. W. Hill, and R. A. Dryfe, *ACS Nano*, **5**, 8809 (2011).
113. A. G. Guell, A. S. Cuharuc, Y. R. Kim, G. Zhang, S. Y. Tan, N. Ebejer, and P. R. Unwin, *ACS Nano*, **9**, 3558 (2015).
114. D. A. Brownson and C. E. Banks, *Phys. Chem. Chem. Phys.*, **14**, 8264 (2012).
115. R. L. McCreery, *Chem. Rev.*, **108**, 2646 (2008).
116. P. Chen and R. L. McCreery, *Anal. Chem.*, **68**, 3958 (1996).
117. C. Anichini, W. Czepa, D. Pakulski, A. Aliprandi, A. Ciesielski, and P. Samorì, *Chem. Soc. Rev.*, **47**, 4860 (2018).
118. J. Wang, *Chem. Rev.*, **108**, 814 (2008).
119. G. E. Fenoy, W. A. Marmisolle, O. Azzaroni, and W. Knoll, *Biosens. Bioelectron.*, **148**, 111796 (2020).
120. S. Rumyantsev, G. Liu, M. S. Shur, R. A. Potyrailo, and A. A. Balandin, *Nano Lett.*, **12**, 2294 (2012).
121. R. Hajian et al., *Nat. Biomed. Eng.*, **3**, 427 (2019).
122. S. Myung, P. T. Yin, C. Kim, J. Park, A. Solanki, P. I. Reyes, Y. Lu, K. S. Kim, and K.-B. Lee, *Adv. Mater.*, **24**, 6081 (2012).
123. Y. Wang, Y. Bi, R. Wang, L. Wang, H. Qu, and L. Zheng, *J. Agric. Food Chem.*, **69**, 1398 (2021).
124. Z. Hao, Y. Zhu, X. Wang, P. G. Rotti, C. DiMarco, S. R. Tyler, X. Zhao, J. F. Engelhardt, J. Hone, and Q. Lin, *ACS Appl. Mater. Interfaces*, **9**, 27504 (2017).
125. H. E. Kim, A. Schuck, J. H. Lee, and Y.-S. Kim, *Sens. Actuators, B*, **291**, 96 (2019).
126. H. H. Bay, R. Vo, X. Dai, H.-H. Hsu, Z. Mo, S. Cao, W. Li, F. G. Omenetto, and X. Jiang, *Nano Lett.*, **19**, 2620 (2019).
127. K. Nagashio, T. Nishimura, K. Kita, and A. Toriumi, *IEEE Int. Electron Devices Meet. (IEDM)*, 1 (2009).
128. K. Nagashio, T. Nishimura, K. Kita, and A. Toriumi, *Appl. Phys. Lett.*, **97**, 143514 (2010).
129. F. Xia, V. Perebeinos, Y.-M. Lin, Y. Wu, and P. Avouris, *Nat. Nanotechnol.*, **6**, 179 (2011).
130. E. Watanabe, A. Conwill, D. Tsuya, and Y. Koide, *Diamond Relat. Mater.*, **24**, 171 (2012).
131. H. Y. Park et al., *Adv. Mater.*, **28**, 864 (2016).
132. G. Giovannetti, P. A. Khomyakov, G. Brocks, V. M. Karpan, J. van den Brink, and P. J. Kelly, *Phys. Rev. Lett.*, **101**, 026803 (2008).
133. F. Léonard and A. A. Talin, *Nat. Nanotechnol.*, **6**, 773 (2011).
134. C. Gong, G. Lee, B. Shan, E. M. Vogel, R. M. Wallace, and K. Cho, *J. Appl. Phys.*, **108**, 123711 (2010).
135. M. S. Choi, S. H. Lee, and W. J. Yoo, *J. Appl. Phys.*, **110**, 073305 (2011).
136. D. Berdebes, T. Low, Y. Sui, J. Appenzeller, and M. S. Lundstrom, *IEEE Trans. Electron Devices*, **58**, 3925 (2011).
137. J. S. Moon et al., *Appl. Phys. Lett.*, **100**, 203512 (2012).
138. J. T. Smith, A. D. Franklin, D. B. Farmer, and C. D. Dimitrakopoulos, *ACS Nano*, **7**, 3661 (2013).
139. J. A. Robinson, M. LaBella, M. Zhu, M. Hollander, R. Kasarda, Z. Hughes, K. Trumbull, R. Cavalero, and D. Snyder, *Appl. Phys. Lett.*, **98**, 053103 (2011).
140. B. Hoefflinger, "ITRS: The International Technology Roadmap for Semiconductors." *Chips 2020* (Springer, Heidelberg) (2012).
141. B. Huard, N. Stander, J. A. Sulpizio, and D. Goldhaber-Gordon, *Phys. Rev. B*, **78**, 121402 (2008).
142. C. E. Malec, B. Elkus, and D. Davidovic, *Solid State Commun.*, **151**, 1791 (2011).
143. W. S. Leong, C. T. Nai, and J. T. Thong, *Nano Lett.*, **14**, 3840 (2014).
144. O. Balci and C. Kocabas, *Appl. Phys. Lett.*, **101**, 243105 (2012).
145. W. Li, C. A. Hacker, G. Cheng, Y. Liang, B. Tian, A. R. H. Walker, C. A. Richter, D. J. Gundlach, X. Liang, and L. Peng, *J. Appl. Phys.*, **115**, 114304 (2014).
146. V. Passi, A. Gahoi, E. G. Marin, T. Cusati, A. Fortunelli, G. Iannaccone, G. Fiori, and M. C. Lemme, *Adv. Mater. Interfaces*, **6**, 1801285 (2019).
147. F. Liu, W. T. Navaraj, N. Yogeswaran, D. H. Gregory, and R. Dahiya, *ACS Nano*, **13**, 3257 (2019).
148. E. Stern, R. Wagner, F. J. Sigworth, R. Breaker, T. M. Fahmy, and M. A. Reed, *Nano Lett.*, **7**, 3405 (2007).
149. G.-J. Zhang, G. Zhang, J. H. Chua, R.-E. Chee, E. H. Wong, A. Agarwal, K. D. Buddharaju, N. Singh, Z. Gao, and N. Balasubramanian, *Nano Lett.*, **8**, 1066 (2008).
150. S. Sorgenfrei, C. Y. Chiu, M. Johnston, C. Nuckolls, and K. L. Shepard, *Nano Lett.*, **11**, 3739 (2011).
151. J. N. Israelachvili, *Intermolecular and Surface Forces* (Academic press, USA) (2011)9780123919274.
152. K. Maehashi, T. Katsura, K. Kerman, Y. Takamura, K. Matsumoto, and E. Tamiya, *Anal. Chem.*, **79**, 782 (2007).
153. N. Gao, T. Gao, X. Yang, X. Dai, W. Zhou, A. Zhang, and C. M. Lieber, *Proc. Natl. Acad. Sci. U. S. A.*, **113**, 14633 (2016).
154. W. Huang, A. K. Diallo, J. L. Dailey, K. Besar, and H. E. Katz, *J. Mater. Chem. C*, **3**, 6445 (2015).
155. T. Ono, Y. Kanai, K. Inoue, Y. Watanabe, S. Nakakita, T. Kawahara, Y. Suzuki, and K. Matsumoto, *Nano Lett.*, **19**, 4004 (2019).
156. M. T. Hwang et al., *Nat. Commun.*, **11**, 1543 (2020).
157. J. O. M. Bockris, E. Gileadi, and K. Müller, *J. Chem. Phys.*, **44**, 1445 (1966).
158. I. Novodchuk, M. Bajcsy, and M. Yavuz, *Carbon*, **172**, 431 (2021).
159. V. Georgakilas, M. Otyepka, A. B. Bourlinos, V. Chandra, N. Kim, K. C. Kemp, P. Hobza, R. Zboril, and K. S. Kim, *Chem. Rev.*, **112**, 6156 (2012).
160. J. E. Johns and M. C. Hersam, *Acc. Chem. Res.*, **46**, 77 (2013).
161. S. L. Wong, H. Huang, Y. Wang, L. Cao, D. Qi, I. Santoso, W. Chen, and A. T. Wee, *ACS Nano*, **5**, 7662 (2011).
162. R. R. Nair et al., *Small*, **6**, 2877 (2010).
163. E. Bekyarova, S. Sarkar, S. Niyogi, M. E. Itkis, and R. C. Haddon, *J. Phys. D: Appl. Phys.*, **45**, 154009 (2012).
164. J. T. Robinson et al., *Nano Lett.*, **10**, 3001 (2010).
165. H. Y. Mao, Y. H. Lu, J. D. Lin, S. Zhong, A. T. S. Wee, and W. Chen, *Prog. Surf. Sci.*, **88**, 132 (2013).
166. S. Islam, S. Shukla, V. K. Bajpai, Y. K. Han, Y. S. Huh, A. Kumar, A. Ghosh, and S. Gandhi, *Biosens. Bioelectron.*, **126**, 792 (2019).
167. Z. Tehrani, G. Burwell, M. A. M. Azmi, A. Castaing, R. Rickman, J. Almarashi, P. Dunstan, A. M. Beigi, S. H. Doak, and O. J. Guy, *2D Mater.*, **1**, 025004 (2014).
168. A. Sinitskii, A. Dimiev, D. A. Corley, A. A. Fursina, D. V. Kosynkin, and J. M. Tour, *ACS Nano*, **4**, 1949 (2010).
169. D. C. Elias et al., *Science*, **323**, 610 (2009).
170. V. Georgakilas, J. N. Tiwari, K. C. Kemp, J. A. Perman, A. B. Bourlinos, K. S. Kim, and R. Zboril, *Chem. Rev.*, **116**, 5464 (2016).
171. W. Fu, C. Nef, A. Tarasov, M. Wipf, R. Stoop, O. Knopfmacher, M. Weiss, M. Calame, and C. Schonenberger, *Nanoscale*, **5**, 12104 (2013).
172. L. P. Chen, L. J. Wang, Z. G. Shuai, and D. Beljonne, *J. Phys. Chem. Lett.*, **4**, 2158 (2013).
173. J. H. An, S. J. Park, O. S. Kwon, J. Bae, and J. Jang, *ACS Nano*, **7**, 10563 (2013).

174. S. Bose, T. Kuila, A. K. Mishra, N. H. Kim, and J. H. Lee, *Nanotechnology*, **22**, 405603 (2011).
175. H. Ni, F. Xu, A. P. Tomsia, E. Saiz, L. Jiang, and Q. Cheng, *ACS Appl. Mater. Interfaces*, **9**, 24987 (2017).
176. A. B. Bourlinos, V. Georgakilas, R. Zboril, T. A. Steriotis, and A. K. Stubos, *Small*, **5**, 1841 (2009).
177. F. Karlicky, K. Kumara Ramanatha Datta, M. Otyepka, and R. Zboril, *ACS Nano*, **7**, 6434 (2013).
178. S. K. Min, W. Y. Kim, Y. Cho, and K. S. Kim, *Nat. Nanotechnol.*, **6**, 162 (2011).
179. M. B. Ebrahim-Habibi, M. Ghobeh, F. A. Mahyari, H. Rafii-Tabar, and P. Sasanpour, *Sci. Rep.*, **9**, 1273 (2019).
180. L. Wang, Y. Zhang, A. Wu, and G. Wei, *Anal. Chim. Acta*, **985**, 24 (2017).
181. D. Mudusu, K. R. Nandanapalli, S. Lee, and Y.-B. Hahn, *Adv. Colloid Interface Sci.*, **283**, 102225 (2020).
182. T. T. Tran and A. Mulchandani, *TrAC, Trends Anal. Chem.*, **79**, 222 (2016).
183. J. Ping, R. Vishnubhotla, A. Vrudhula, and A. T. C. Johnson, *ACS Nano*, **10**, 8700 (2016).
184. Y. Liu, Y. Huang, and X. Duan, *Nature*, **567**, 323 (2019).
185. K. Autumn, M. Sitti, Y. A. Liang, A. M. Peattie, W. R. Hansen, S. Sponberg, T. W. Kenny, R. Fearing, J. N. Israelachvili, and R. J. Full, *Proc. Natl. Acad. Sci. U. S. A.*, **99**, 12252 (2002).
186. A. K. Geim, S. V. Dubonos, I. V. Grigorieva, K. S. Novoselov, A. A. Zhukov, and S. Y. Shapoval, *Nat. Mater.*, **2**, 461 (2003).
187. Z. Wang, Z. Hao, S. Yu, C. G. De Moraes, L. H. Suh, X. Zhao, and Q. Lin, *Adv. Funct. Mater.*, **29**, 1905202 (2019).
188. S. Guo, S. Zhang, and S. Sun, *Angew. Chem. Int. Ed. Engl.*, **52**, 8526 (2013).
189. J. Liu, Q. Ma, Z. Huang, G. Liu, and H. Zhang, *Adv. Mater.*, **31**, 1800696 (2019).
190. M. D. Stoller, S. Park, Y. Zhu, J. An, and R. S. Ruoff, *Nano Lett.*, **8**, 3498 (2008).
191. Y. Xiao, F. Patolsky, E. Katz, J. F. Hainfeld, and I. Willner, *Science*, **299**, 1877 (2003).
192. G. Peng, U. Tisch, O. Adams, M. Hakim, N. Shehada, Y. Y. Broza, S. Billan, R. Abdah-Bortnyak, A. Kuten, and H. Haick, *Nat. Nanotechnol.*, **4**, 669 (2009).
193. J. Luo, S. Jiang, H. Zhang, J. Jiang, and X. Liu, *Anal. Chim. Acta*, **709**, 47 (2012).
194. D. Wang, X. Liu, L. He, Y. Yin, D. Wu, and J. Shi, *Nano Lett.*, **10**, 4989 (2010).
195. J. M. Tour, L. Jones, D. L. Pearson, J. J. Lamba, T. P. Burgin, G. M. Whitesides, D. L. Allara, A. N. Parikh, and S. Atre, *J. Am. Chem. Soc.*, **117**, 9529 (1995).
196. E. Danielson et al., *Biosens. Bioelectron.*, **165**, 112419 (2020).
197. Y. Wu et al., *Small*, **8**, 3129 (2012).
198. Z. Gao et al., *ACS Appl. Mater. Interfaces*,, **8**, 27546 (2016).
199. K. S. Subrahmanyam, A. K. Manna, S. K. Pati, and C. N. R. Rao, *Chem. Phys. Lett.*, **497**, 70 (2010).
200. J. Lee, K. S. Novoselov, and H. S. Shin, *ACS Nano*, **5**, 608 (2011).
201. F. Jimenez-Villacorta, E. Climent-Pascual, R. Ramirez-Jimenez, J. Sanchez-Marcos, C. Prieto, and A. de Andres, *Carbon*, **101**, 305 (2016).
202. G. Xu, J. Liu, Q. Wang, R. Hui, Z. Chen, V. A. Maroni, and J. Wu, *Adv. Mater.*, **24**, 71 (2012).
203. F. Yan, M. Zhang, and J. Li, *Adv. Healthcare Mater.*, **3**, 313 (2014).
204. F. Liu, Y. H. Kim, D. S. Cheon, and T. S. Seo, *Sens. Actuators, B*, **186**, 252 (2013).
205. Y. Chen, R. Ren, H. Pu, X. Guo, J. Chang, G. Zhou, S. Mao, M. Kron, and J. Chen, *Sci. Rep.*, **7**, 10974 (2017).
206. B. Cai, L. Huang, H. Zhang, Z. Sun, Z. Zhang, and G.-J. Zhang, *Biosens. Bioelectron.*, **74**, 329 (2015).
207. H. M. Li, Y. H. Zhu, M. S. Islam, M. A. Rahman, K. B. Walsh, and G. Koley, *Sens. Actuators, B*, **253**, 759 (2017).
208. Y. X. Huang, X. C. Dong, Y. M. Shi, C. M. Li, L. J. Li, and P. Chen, *Nanoscale*, **2**, 1485 (2010).
209. Y. Ohno, K. Maehashi, and K. Matsumoto, *J. Am. Chem. Soc.*, **132**, 18012 (2010).
210. Y. Ohno, K. Maehashi, Y. Yamashiro, and K. Matsumoto, *Nano Lett.*, **9**, 3318 (2009).
211. X. Dong, Y. Shi, W. Huang, P. Chen, and L. J. Li, *Adv. Mater.*, **22**, 1649 (2010).
212. F. Traversi, C. Raillon, S. M. Benameur, K. Liu, S. Khlybov, M. Tosun, D. Krasnozhon, A. Kis, and A. Radenovic, *Nat. Nanotechnol.*, **8**, 939 (2013).
213. B. J. Cai, S. T. Wang, L. Huang, Y. Ning, Z. Y. Zhang, and G. J. Zhang, *ACS Nano*, **8**, 2632 (2014).
214. C. Zheng, L. Huang, H. Zhang, Z. Sun, Z. Zhang, and G. J. Zhang, *ACS Appl. Mater. Interfaces*, **7**, 16953 (2015).
215. D. K. Ban et al., *ACS Nano*, **14**, 6743 (2020).
216. W. Fu, L. Feng, D. Mayer, G. Panaitov, D. Kireev, A. Offenhäusser, and H.-J. Krause, *Nano Lett.*, **16**, 2295 (2016).
217. Y. Sun, S. Xu, T. Zhu, J. Lu, S. Chen, M. Liu, G. Wang, B. Man, H. Li, and C. Yang, *Carbon*, **182**, 167 (2021).
218. K. Mensah, I. Cissé, A. Pierret, M. Rosticher, J. Palomo, P. Morfin, B. Plaçais, and U. Bockelmann, *Adv. Healthcare Mater.*, **9**, 2000260 (2020).
219. Z. Gao et al., *Nano Lett.*, **18**, 3509 (2018).
220. S. Xu et al., *Nat. Commun.*, **8**, 14902 (2017).
221. R. Campos, J. Borme, J. R. Guerreiro, G. Machado, M. F. Cerqueira, D. Y. Petrovykh, and P. Alpuim, *ACS Sens.*, **4**, 286 (2019).
222. S. Xu et al., *Appl. Surf. Sci.*, **427**, 1114 (2018).
223. Y. Xia, Y. Sun, H. Li, S. Chen, T. Zhu, G. Wang, B. Man, J. Pan, and C. Yang, *Talanta*, **223**, 121766 (2021).
224. J. Gao, Y. Gao, Y. Han, J. Pang, C. Wang, Y. Wang, H. Liu, Y. Zhang, and L. Han, *ACS Appl. Electron. Mater.*, **2**, 1090 (2020).
225. M. B. Lerner et al., *Sens. Actuators, B*, **239**, 1261 (2017).
226. X. Wang, Y. Zhu, T. R. Olsen, N. Sun, W. Zhang, R. Pei, and Q. Lin, *Electrochim. Acta*, **290**, 356 (2018).
227. S. Gao, R. Wang, Y. Bi, H. Qu, Y. Chen, and L. Zheng, *Sens. Actuators, B*, **305**, 127167 (2020).
228. D. H. Shin, W. Kim, J. Jun, J. S. Lee, J. H. Kim, and J. Jang, *Sens. Actuators, B*, **264**, 216 (2018).
229. C. Xiong, T. Zhang, W. Kong, Z. Zhang, H. Qu, W. Chen, Y. Wang, L. Luo, and L. Zheng, *Biosens. Bioelectron.*, **101**, 21 (2018).
230. G. Seo et al., *ACS Nano*, **14**, 12257 (2020).
231. Y. Li et al., *ACS Omega*, **6**, 6643 (2021).
232. S. Afsahi et al., *Biosens. Bioelectron.*, **100**, 85 (2018).
233. L. Zhou et al., *Biosens. Bioelectron.*, **87**, 701 (2017).
234. S. Ramadan et al., *ACS Appl. Mater. Interfaces*, **13**, 7854 (2021).
235. N. Kumar et al., *Biosens. Bioelectron.*, **156**, 112123 (2020).
236. Z. Gao et al., *2D Mater.*, **7**, 024001 (2020).
237. S. Kim et al., *ACS Appl. Mater. Interfaces*, **11**, 13927 (2019).
238. S. Wang, M. Z. Hossain, K. Shinozuka, N. Shimizu, S. Kitada, T. Suzuki, R. Ichige, A. Kuwana, and H. Kobayashi, *Biosens. Bioelectron.*, **165**, 112363 (2020).
239. S. Xu et al., *Sens. Actuators, B*, **284**, 125 (2019).
240. Y. Kanai, Y. Ohmuro-Matsuyama, M. Tanioku, S. Ushiba, T. Ono, K. Inoue, T. Kitaguchi, M. Kimura, H. Ueda, and K. Matsumoto, *ACS Sens.*, **5**, 24 (2020).
241. S. Liu, Y. Fu, C. Xiong, Z. Liu, L. Zheng, and F. Yan, *ACS Appl. Mater. Interfaces*, **10**, 23522 (2018).
242. S. Xu, C. Zhang, S. Jiang, G. Hu, X. Li, Y. Zou, H. Liu, J. Li, Z. Li, X. Wang, M. Li, and J. Wang et al., *Sens. Actuators, B*, **326**, 128991 (2021).
243. R. Wang, Y. Mao, L. Wang, H. Qu, Y. Chen, and L. Zheng, *Food Chem.*, **347**, 128980 (2021).
244. T. Tao, Y. Zhou, M. Ma, H. He, N. Gao, Z. Cai, G. Chang, and Y. He, *Sens. Actuators, B*, **328**, 128936 (2021).
245. X. Shang, C. H. Park, G. Y. Jung, S. K. Kwak, and J. H. Oh, *ACS Appl. Mater. Interfaces*, **10**, 36194 (2018).
246. A. Schuck, H. E. Kim, K.-M. Jung, W. Hasenkamp, and Y.-S. Kim, *Biosens. Bioelectron.*, **157**, 112167 (2020).
247. S. R. Ahn, J. H. An, H. S. Song, J. W. Park, S. H. Lee, J. H. Kim, J. Jang, and T. H. Park, *ACS Nano*, **10**, 7287 (2016).
248. WHO, Ten threats to global health in 2019, 2019, https://who.int/news-room/spotlight/ten-threats-to-global-health-in-2019.
249. S. Wang, L. Zhao, R. Xu, Y. Ma, and L. Ma, *J. Electroanal. Chem.*, **853**, 113527 (2019).
250. R. Kalluri and S. LeBleu Valerie, *Science*, **367**, eaau6977 (2020).
251. G. A. Martini, *Postgrad. Med. J.*, **49**, 542 (1973).
252. A. S. Fauci, *Science*, **239**, 617 (1988).
253. S. K. P. Lau, P. C. Y. Woo, K. S. M. Li, Y. Huang, H.-W. Tsoi, B. H. L. Wong, S. S. Y. Wong, S.-Y. Leung, K.-H. Chan, and K.-Y. Yuen, *Proc. Natl. Acad. Sci. U. S. A.*, **102**, 14040 (2005).
254. A. Assiri et al., *N. Engl. J. Med.*, **369**, 407 (2013).
255. G. Pialoux, B. A. Gauzere, S. Jaureguiberry, and M. Strobel, *Lancet Infect. Dis.*, **7**, 319 (2007).
256. D. B. Lewis, *Annu. Rev. Med.*, **57**, 139 (2006).
257. B. J. Coburn, B. G. Wagner, and S. Blower, *BMC Med.*, **7**, 30 (2009).
258. M. R. Duffy et al., *N. Engl. J. Med.*, **360**, 2536 (2009).
259. P. Zhou et al., *Nature*, **579**, 270 (2020).
260. E. Masvidal-Codina et al., *Nat. Mater.*, **18**, 280 (2019).
261. Y. Zhang, X. Liu, S. Qiu, Q. Zhang, W. Tang, H. Liu, Y. Guo, Y. Ma, X. Guo, and Y. Liu, *J. Am. Chem. Soc.*, **141**, 14643 (2019).
262. R. Garcia-Cortadella et al., *Small*, **16**, 1906640 (2020).
263. B. M. Blaschke et al., *2D Mater.*, **4**, 025040 (2017).
264. C. A. Clifford, E. H. Martins Ferreira, T. Fujimoto, J. Herrmann, A. R. Hight Walker, D. Koltsov, C. Punckt, L. Ren, G. J. Smallwood, and A. J. Pollard, *Nat. Rev. Phys.*, **3**, 233 (2021).
265. S. Milana, *Nat. Phys.*, **17**, 1068 (2021).
266. B. R. Goldsmith et al., *Sci. Rep.*, **9**, 434 (2019).
267. A. Rajkomar, J. Dean, and I. Kohane, *N. Engl. J. Med.*, **380**, 1347 (2019).
268. M. Mujeeb-U-Rahman, M. Honarvar, Nazari, and M. Sencan, *Biosens. Bioelectron.*, **124–125**, 66 (2019).
269. R. M. Torrente-Rodríguez et al., *Matter*, **2**, 921 (2020).